

Handling Qualities Flight Test Assessment of a Business Jet N_zU P - β Fly-By-Wire Control System

Tom Berger* and Mark B. Tischler†

Steven G. Hagerott‡

U.S. Army Aviation Development Directorate, Moffett Field, CA

Textron Aviation, Wichita, KS

M. Christopher Cotting§, Capt James L. Gresham¶, Capt Justin E. George||,
Capt Kyle J. Krogh||, 1st Lt Alessandro D'Argenio¶ and Capt Justin D. Howland¶

USAF Test Pilot School, Edwards AFB, CA

Fly-by-wire control laws for a business jet were developed and a handling qualities assessment flight test was conducted on the Calspan Variable Stability System Learjet-25. The control laws, which provide an n_zu -command response type in the longitudinal axis and a p - β -command response type in the lateral/directional axes, were optimized to meet Level 1 requirements for a comprehensive set of stability, handling qualities, and performance specifications. The control laws were evaluated in flight by USAF Test Pilot School and Textron Aviation test pilots using a series of handling qualities demonstration maneuvers. These included pitch and roll capture and tracking tasks and an offset landing task. Quantitative performance metrics were collected, in addition to pilot handling qualities ratings and comments. Several modifications were made to the control laws based on initial pilot comments and ratings. The final results show that the optimized fly-by-wire control laws provided assigned Level 1 handling qualities for discrete tracking and offset landing tasks.

I. Introduction

SEVERAL comprehensive compendiums of flight control design experience and lessons learned emphasize the importance of meeting a multi-tiered set of handling qualities and flight control requirements for improved safety (e.g., RTO,¹ Pratt,² Tischler et al³). Ref. 1 mentions this approach as a best practice for flight control design and suggests that pilot induced oscillations (PIO), or aircraft pilot coupling (APC), could be avoided in the design phase by exploiting handling-qualities criteria to design for good handling qualities. It also suggests using supplementary criteria where necessary, in addition to the military specifications. Many of these supplementary criteria, such as the bandwidth criteria⁴ and the Gibson criteria,⁵ have been incorporated into the latest version of military specification MIL-STD-1797B.⁶ More recently, Balas and Hodgkinson⁷ also referred to different tiers of requirements, or alternate criteria, used to supplement the equivalent modal parameter requirements.

Such a handling qualities optimization-based approach to flight control design was previously developed and used to design fly-by-wire (FBW) control laws for a business jet similar to a Cessna CitationJet CJ1.^{8,9} The control laws were tested in a fixed-based simulation environment.¹⁰ The results from the simulation handling-qualities assessment showed overall Level 1 handling qualities, and the control laws were rated as very predictable and pilots could be more aggressive with a higher level of precision than with the bare-airframe. The control system optimization, conducted using the Control Designer's Unified Interface

*Aerospace Engineer, Senior Member AIAA.

†Flight Control Technology Group Leader, Senior Scientist, Associate Fellow AIAA.

‡Senior Engineer Specialist, Senior Member AIAA.

§Master Instructor of Flying Qualities, Associate Fellow AIAA.

¶Experimental Flight Test Engineer, Member AIAA.

||Experimental Test Pilot, Member AIAA.

Distribution Statement A: Approved for public release; distribution is unlimited. 412 TW-PA-17011

(CONDUIT[®]),¹¹ was driven by a comprehensive set of specifications divided into two tiers: Tier 1 specifications were used to drive the optimization, and Tier 2 specifications were used to check many commonly used alternative requirements for the completed design.

As with the development of any new control system, the aircraft needs to be evaluated using high-gain, pilot-in-the-loop flight-test tasks to ensure that the predicted handling-qualities Level has been achieved,⁶ and that no handling-qualities “cliffs” are present. Therefore, in the current study, the methods developed and tested in the previous CJ1 simulation study were applied to and evaluated in a flight test on the Calspan Variable Stability System (VSS) Learjet LJ-25D.

The handling-qualities flight-test assessment was conducted at the USAF Test Pilot School (TPS), Edwards AFB, CA, with the following four objectives. First, to evaluate and quantify the handling qualities of the FBW control laws, in order to validate the optimization approach used for flight control design. Second, to ensure that the closed-loop handling characteristics exhibit classical airplane response types that do not require pilot re-training or adaptation, and to verify that the control laws do not exhibit any unusual responses or PIO tendencies while performing operationally relevant as well as high gain tasks. Third, to quantify the benefits of the FBW control system over the bare-airframe. And finally, to ensure that the control design methods previously demonstrated on the CJ1 aircraft are generic and will work for the LJ-25. The tasks used to demonstrate these objectives in flight were selected from MIL-STD-1797B⁶ and an Air Force technical report cataloging handling qualities maneuvers for fixed-wing aircraft (WL-TR-97-3100),¹² and include such tasks as offset landing and pitch and roll tracking.

The remainder of the paper covers a description of the test aircraft, its flight and loading envelopes, and the design points used to develop the control law gain schedule (Section II). Section III provides an overview of the control law optimization technique used, which accounts for off-nominal loading conditions at each design point. Next, a review of the $n_z u$ and p - β architectures is provided, along with a comprehensive list of specifications used for control law optimization in each axis. Example optimization results are given at one flight condition, which show the predicted Level 1 handling qualities for Tier 1 and Tier 2 specifications. A validation of the integrated control system is shown against the analysis model used for control law optimization in Section IV. This is followed by the details of the handling qualities test maneuvers and results of the handling qualities assessment flight test. Finally, conclusions are provided based on the results of the flight test

II. Test Aircraft

The aircraft used for this flight test is the Calspan Variable Stability System (VSS) Learjet LJ-25D, shown in Figure 1. It is a twin turbojet-powered business jet, which in its unmodified state can carry eight passengers. It has a maximum take-off weight (MTOW) of 15,000 lbs, a cruise speed of 464 KTAS, a maximum range of 1,535 nm, and a service ceiling of 45,000 ft. The VSS allows for in-flight simulation of different aircraft control laws and responses in four degrees-of-freedom. For this test, the VSS was used to run the FBW control laws described in Section III.

The aircraft was manned by a safety pilot (SP) in the left seat and an evaluation pilot (EP) in the right seat during all operations. A Head Down Display (HDD) was mounted on the right instrument panel in front of the EP and was capable of displaying a tracking program used to evaluate handling qualities.

An accurate model of the Learjet was developed¹⁴ as a basis for the control law design and optimization. The full flight-envelope stitched¹³ simulation model of the Learjet was developed from an eight-hour flight-test program with four identified point models and trim data, and used for control law design and optimization. The model allows for accurate interpolation in airspeed, altitude, and flaps, and extrapolation in weight, inertia, and CG location. Berger et al.¹⁴ details the development and validation of the Learjet stitched model.

Linear state-space models were extracted from the stitched model for control law design at 66 flight conditions (Figure 2) and 14 loading configurations (Figure 3) spanning the aircraft envelopes.¹⁵ The following section will describe the control laws in more detail.



Figure 1. Calspan Variable Stability System Learjet LJ-25D.

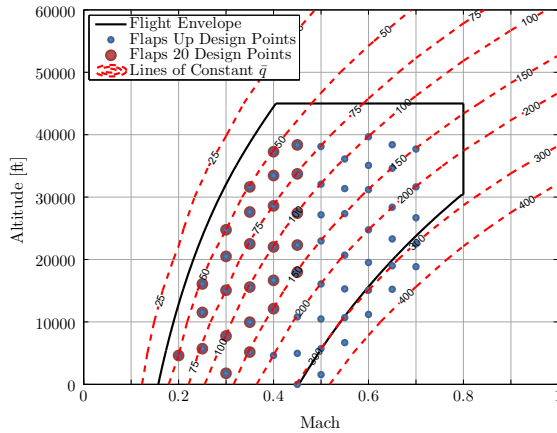


Figure 2. Aircraft flight envelope and flight condition design points used in control laws development.

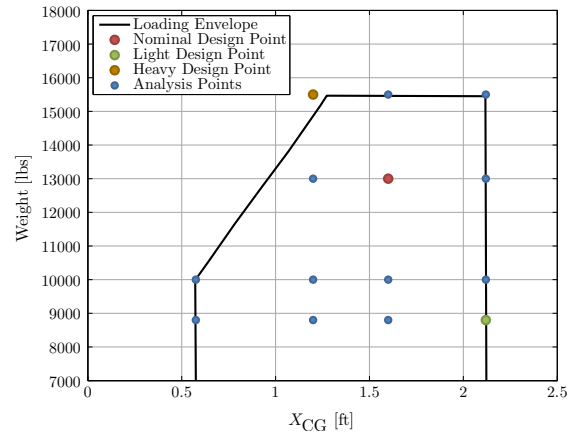


Figure 3. Aircraft loading envelope and loading configurations design and analysis points used in control laws development.

III. Control Laws

The control laws used in this study are based on those previously developed for a small business jet similar to a Cessna CitationJet CJ1^{8,9} and tested in a simulation handling qualities evaluation.¹⁰ The control laws are based on an architecture that is analogous to an explicit model following system,¹⁶ implemented to provide an “ $n_z u$ ”-command¹⁷ response type in the longitudinal axis (Section III.A) and a “ p - β ”-command^{18,19} response type in the lateral/directional axes (Section III.B).

The control law parameters (i.e., feedback gains, feed-forward gains, and command model parameters) were gain scheduled with flight condition. To determine the gain schedule and adequately cover the flight envelope, models at 66 different Mach and dynamics pressure combinations, shown in Figure 2, were used as design points in the control law optimization. In addition, since the control laws are also scheduled with flaps, 26 Mach/dynamics pressure design points were repeated for a powered approach configurations (flaps 20), also shown in Figure 2.

At each of the 66 flaps up and 26 flaps down (92 total) design points (flight conditions), the control laws were optimized in CONDUIT[®] using a multi-objective parametric optimization method¹¹ that directly tunes the design parameters (feedback gains) to meet a total of 52 specifications. The feasible sequential quadratic programming (FSQP) optimization algorithm proved capable of determining a smooth gain schedule which concurrently met the large number of frequency- and time-domain specifications for both nominal and off-nominal models, while minimizing over-design. These are the *Pareto optimal solutions* for each of the 92 design points, which meet all specifications with the most economical use of actuators while minimizing sensitivity to noise. Tables listing the specifications used are provided in Section III.A for the longitudinal

axis and Section III.B for the lateral/directional axes.

Furthermore, at each of the 92 design points (flight conditions), the performance robustness of the control laws was ensured by using a *multi-model optimization approach* which requires key specifications to be met for edge-of-the-envelope weight/CG configurations (labeled as “Heavy” and “Light” in Figure 3) in addition to the nominal loading configuration (labeled as “Nominal” in Figure 3). Performance robustness was also ensured by enforcing a minimum broken-loop crossover frequency in each control law axis. This allowed the scheduling of the optimized control laws solely with Mach and dynamic pressure resulting in a smooth gain schedule, while still meeting the requirements for the range of weight/CG configurations.^{8,9} At the end of the optimization process, the control law gain schedule performance was evaluated for all 92 flight condition design points and all 14 weight/c.g. loading configuration analysis points to ensure robust predicted Level 1 performance.

The following sections will give a brief overview of the control laws, as well as updates that were made after initial testing.

A. Longitudinal Control Laws

The control law architecture used in the longitudinal axis is shown in simple form in Figure 4. The control laws are referred to as “ $n_z u$ ”-command,^{8,17} i.e., in addition to the stability axes normal acceleration (n_z) command from the pre-filter, a speed error is passed through the feedback integrator (shown in Figure 5). This additional speed error feedback loop provides positive speed stability to the aircraft response, where a pure n_z -command system would otherwise exhibit neutral speed stability. This results in a classical airplane response type with two, frequency-split command types. In the short term ($0.1 < \omega < 10$ rad/sec), the pilot stick commands normal acceleration, while in the long term ($\omega < 0.1$ rad/sec), the pilot stick commands airspeed. The resulting “ $n_z u$ ”-command response type thus preserves the static stability gradients of column

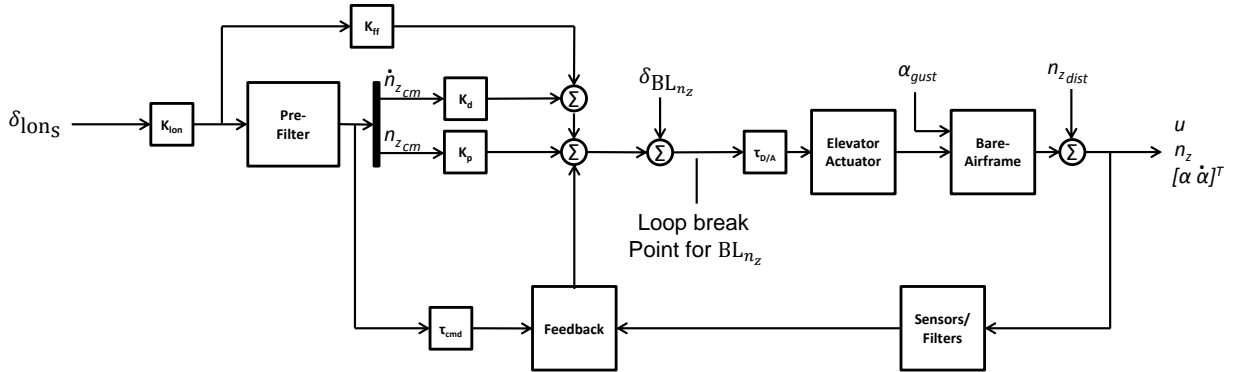


Figure 4. Schematic of longitudinal control law block diagram.

The feed-forward path in the control laws is comprised of the stick gain K_{lon} , pre-filter, and three feed-forward gains (K_{ff} , K_d , and K_p), as shown in Figure 4. The stick gain sets the steady-state column force per g value. The pre-filter acts as a command model and defines the desired short-term aircraft response dynamics, given by:

$$\frac{n_{zcm}}{\delta_{lon_s}} = \frac{K_{lon}\omega_{cm}^2}{s^2 + 2\zeta_{cm}\omega_{cm}s + \omega_{cm}^2} \quad (1)$$

where,

K_{lon} is the stick gain which sets the desired stick force per g ($(F_s/g)_{cm}$),
 ζ_{cm} is set to 1.0 to provide a well damped response, and

ω_{cm} is set to the bare-airframe short-period frequency ω_{sp} to retain the good inherent short-period frequency of the bare-airframe aerodynamic design and to not overdrive the actuators.

Note that the short-period frequency ω_{sp} is selected for the nominal weight/CG configuration (Figure 3, Nominal Design Point), at each flight condition. The remaining elements of the feed-forward path (K_{ff} , K_{d} , and K_{p} gains) take the place of an inverse plant model⁸ and generate the actuator inputs which command the aircraft to approximately follow the command-model response.

A command delay (τ_{cm} block in Figure 4) is added for synchronization of the commanded and measured states in time. Accounting for this additional delay before comparing the commanded states with the measured states is essential to prevent over-driving the actuators. The addition of the equivalent delays also reduces the amount of overshoot in the closed-loop, end-to-end response with no added phase loss for stick input,⁸ and ensures that the zeros introduced by the feed-forward gains follow the closed-loop poles of the plant, independent of feedback gains. This ensures good pole/zero cancellation with low residue, making the command model the dominant dynamics for pilot input.

The feedback path of the control laws (shown in Figure 5) is used to minimize the error between the commanded response and actual aircraft response, as well as to provide improved damping, stability, gust rejection, and robustness. This is done with proportional angle-of-attack and angle-of-attack rate error feedback paths and an integral normal acceleration error and speed error feedback path. As shown in Figure 5, the commanded angle-of-attack α_{cm} and angle-of-attack rate $\dot{\alpha}_{\text{cm}}$ are generated from the commanded normal acceleration $n_{z_{\text{cm}}}$ and normal acceleration rate $\dot{n}_{z_{\text{cm}}}$ by:

$$\alpha_{\text{cm}} = \alpha_{nz} n_{z_{\text{cm}}} \quad (2)$$

$$\dot{\alpha}_{\text{cm}} = \alpha_{nz} \dot{n}_{z_{\text{cm}}} \quad (3)$$

where $\alpha_{nz} = 1/(n/\alpha)$ and n/α is equal to the nominal loading configuration bare-airframe steady-state normal acceleration per angle-of-attack.

The combined normal acceleration error and speed error signal $n_z u_e$ is constructed as:

$$n_z u_e = (n_{z_{\text{cm}}} - n_z) - K_u (V_{\text{ref}} - V_{\text{KCAS}}) \quad (4)$$

where,

$n_{z_{\text{cm}}}$ is the commanded normal acceleration (Equation 1),

n_z is the measured aircraft normal acceleration (in stability axes),

V_{KCAS} is the complementary filtered airspeed in knots of calibrated airspeed (KCAS), and

V_{ref} is the reference airspeed in KCAS controlled by the pilot via the pitch trim switch on the stick.

The speed error gain K_u (Equation 4) sets the desired stick force per knot $(F_s/\text{kt})_{\text{cm}}$, and is equal to:

$$K_u = \frac{(F_s/\text{kt})_{\text{cm}}}{(F_s/g)_{\text{cm}}} \quad (5)$$

The flare characteristics of the control system were perviously tuned in the simulator for the CJ1,¹⁰ by modifying the commanded stick force per knot gradient $(F_s/\text{kt})_{\text{cm}}$, as set in Equation 5, when the landing gear are deployed. The stick force per knot gain (set to 1/6 lb/kt for the normal mode control laws⁸), was increased to 2/3 lb/kt for the flare mode. This increase requires the pilot to pull back more on the stick as the aircraft slows below its reference airspeed before touchdown. A similar increase in the stick force per knot gain was applied to the LJ-25 control laws tested in this flight test.

At each of the 92 flight condition design points (Figure 2), the feedback gains were optimized to meet 21 Tier 1 specifications listed in Table 1. The table also provides the four Tier 2 specifications used as a check at the end of the optimization. Control law performance robustness to changes in weight/CG was provided by enforcing a minimum crossover frequency ($\omega_{c_{n_z}} = 2.5$ rad/sec) for the loop broken at the elevator actuator command (BL_{n_z} , Figure 4). In addition, key specifications (stability and Nichols margins, model following performance, and pitch attitude dropback) were enforced for the Light and Heavy design points (Figure 3) as well as the Nominal design point, in a technique referred to as multi-model optimization.

Figure 6 shows the optimization results for one of the 92 design points—the 250 kts (KCAS), 15,000 ft, flaps up flight condition. All of the Tier 1 specifications are met within the design procedure. Several of

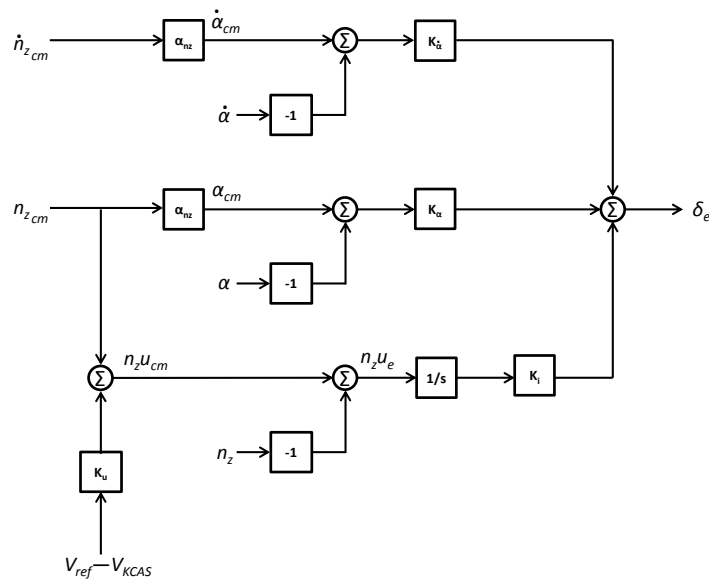


Figure 5. Schematic of longitudinal control law feedback.

the specifications are on the boundary, which is the Pareto optimal solution (i.e., meets the requirements with the minimum “cost of feedback”). Figure 7 shows the $n_z u$ -command frequency response, as well as the aircraft normal acceleration n_z response, for the nominal loading configuration. The responses match well over a wide frequency range, indicating excellent command model following performance. Figure 8 shows the broken-loop frequency response BL_{n_z} , for the loop broken at the elevator actuator. The design is on the minimum crossover frequency requirement ($\omega_{c_{n_z}} = 2.5$ rad/sec) as expected for this Pareto optimal solution, with sufficient stability margins.

Figure 9 shows a 5 sec piloted pulse response, using the short-period dynamics only. The closed-loop aircraft exhibits a classical response with the flight-path response lagging the pitch attitude response by 0.88 sec, equal to the bare-airframe value of $T_{\theta_2} = 0.88$ sec for this flight condition. Figure 10 shows the normal acceleration response to a 1-cosine angle-of-attack gust. The figure shows that the second peak of the nominal configuration response is smaller in magnitude than the first, which is the load alleviation goal enforced by the angle-of-attack gust specification.

Similar results were generated for the remaining 91 design points, which resulted in a smooth gain schedule with predicted Level 1 handling qualities for the full range of flight and loading configurations.

Table 1. Longitudinal Optimization Specifications

Constraint	Spec Name	Description (Motivation)	Domain*	Source	Config.†
<i>Tier 1</i>					
Hard	EigLcG1	Eigenvalues in L.H.P. (Stability)	S	Generic	N
	StbMgG1	Gain Phase Margin broken at elevator (Stability)	F	MIL-DLT-9490E	L,N,H
	NicMgG1	Nichols Margins broken at elevator (Stability)	F	GARTEUR	L,N,H
Soft	CapPiL2	CAP (short-period) (HQ)	L	MIL-STD-1797B	N
	FrqSpL5	ω_{sp} vs n/α (HQ)	L	MIL-STD-1797B	N
	TdlPiL1	Equivalent Time delay (HQ)	L	MIL-STD-1797B	N
	FrqSpC1	$\omega_{sp} \pm 25\%$ open-loop (Act. Activity)	L	Generic	N
	FrqTtC1	$T_{\theta_2} \pm 50\%$ open-loop (HQ, Act. Activity)	L	Generic	N
	CosLoG1	Max LOES Cost ($J \leq 10$) (HQ)	L	Generic	N
	FspGsL1	Stick force per g $\pm 2.5\%$ stick gain (HQ)	F	Generic	N
	FspKtL1	Stick force per kt $\pm 2.5\%$ stick gain (HQ)	F	Generic	N
	ModFoG2	Command model following cost (HQ)	F	Generic	L,N,H
	EigDpG1	Eigenvalue Damping (HQ, Loads)	S	Generic	N
	OlpOpG1	Open Loop Onset Point (PIO)	F	DLR	N
	DrpPiL1	Pitch dropback (HQ)	T	MIL-STD-1797B	L,N,H
	GstRpG1	Angle-of-attack gust response (Loads)	T	Generic	N
	DstBwG1	Dist. Rej. Bandwidth (Loads, Ride Quality)	F	ADS-33E	N
	DstPkG1	Dist. Rej. Peak (Loads, Ride Quality)	F	ADS-33E	N
	CrsMnG1	Minimum $\omega_c \geq 2.5$ rad/sec (Robustness)	F	Generic	N
	Summed	CrsLnG1	Crossover Frequency (Act. Activity)	F	Generic
Obj.	RmsAcG1	Actuator RMS (Act. Activity)	F	Generic	N
<i>Tier 2</i>					
Check Only	BnwPiL4	Pitch attitude bandwidth, phase delay (HQ)	F	MIL-STD-1797B	-
	BnwFpL1	Transient flight-path response (HQ)	F	MIL-STD-1797B	-
	GibPiL1	Gibson phase rate (PIO)	F	AGARD-CP-508	-
	NicMgG1	Nichols Margins broken at sensors (Stability)	F	GARTEUR	-

*F = Frequency domain specification, T = Time domain specification, L = LOES specification, S = s-plane

†N = Nominal weight/CG configuration only, L,N,H = Light, Nominal, and Heavy weight/CG configurations

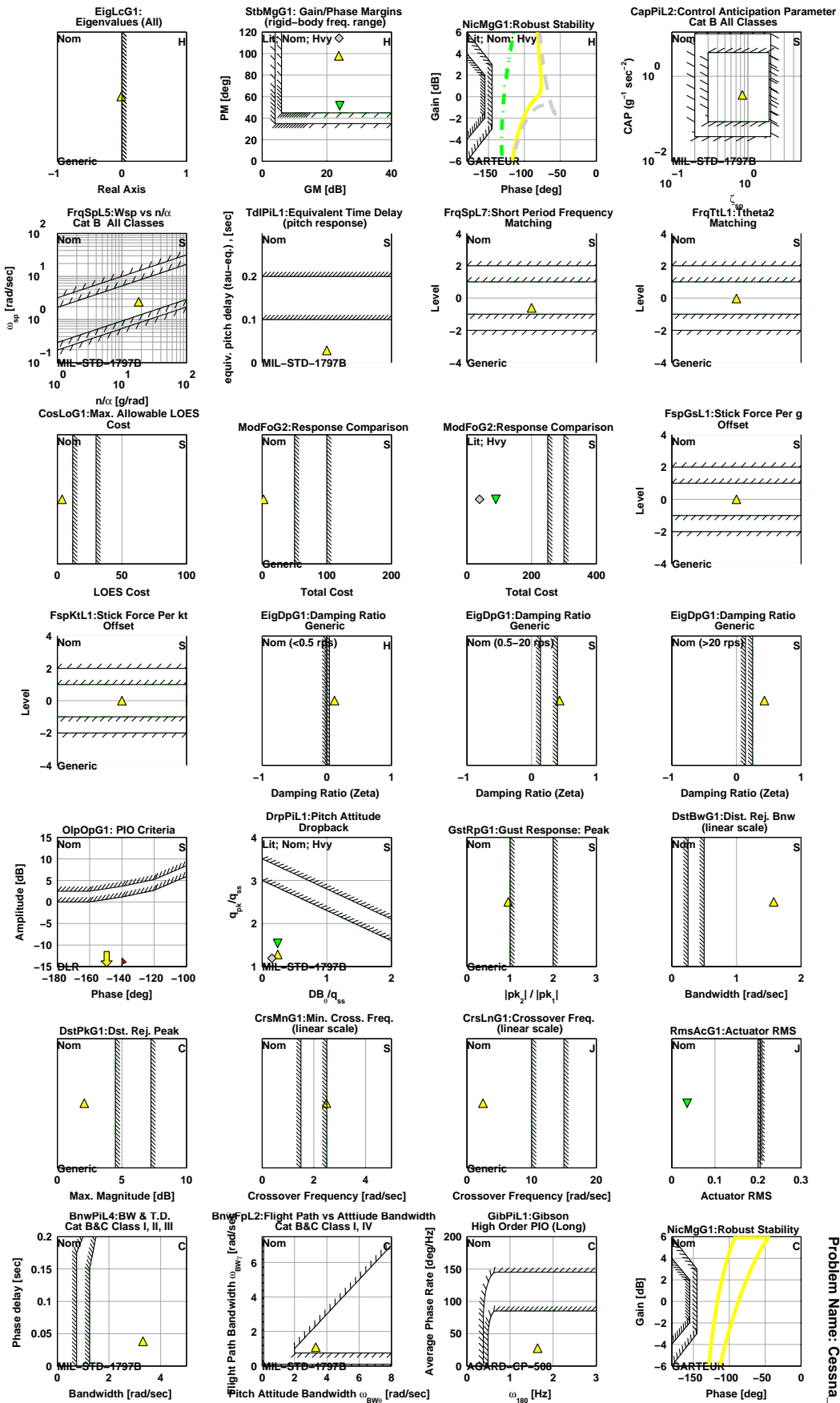


Figure 6. Handling qualities specification results of the optimized design (longitudinal axis, 250 kts, 15,000 ft flight condition).

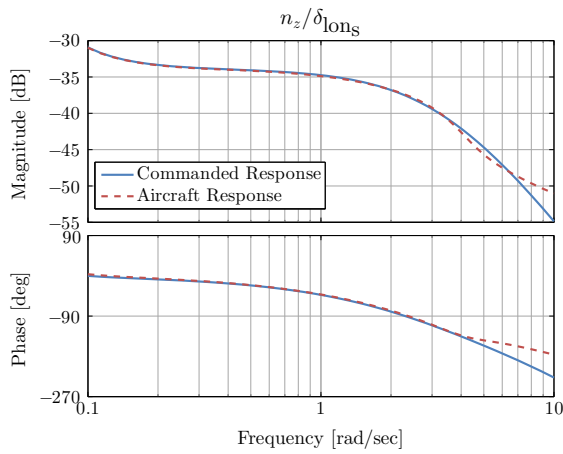


Figure 7. Normal acceleration frequency response (250 kts, 15,000 ft flight condition; Nominal loading configuration).

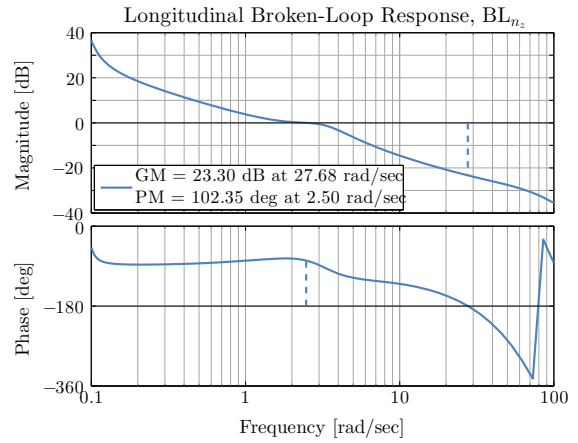


Figure 8. Longitudinal broken-loop (at input to elevator actuator) frequency response (250 kts, 15,000 ft flight condition; Nominal loading configuration).

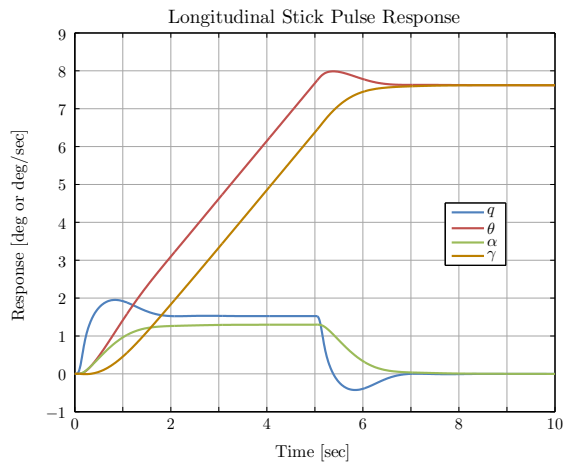


Figure 9. Longitudinal stick 5 sec pulse response (250 kts, 15,000 ft flight condition; Nominal loading configuration; Short-period dynamics only).

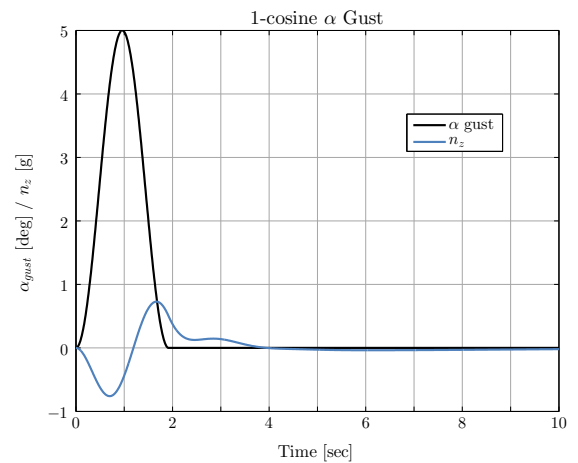


Figure 10. 1-cos angle-of-attack gust response (250 kts, 15,000 ft flight condition; Nominal loading configuration).

B. Lateral/Directional Control Laws

The control law architecture used in the lateral/directional axis is referred to as “ p - β ”-command, i.e., stability axes roll rate command in the lateral axis and sideslip command in the directional axis.^{18,19} The architecture is shown in simple form in Figure 11.

As in the longitudinal axis, the feed-forward paths in the control laws are comprised of the stick gains K_{lat} and K_{ped} , pre-filters, and feed-forward gains (K_{ff} , K_d , and K_p), as shown in Figure 11. The stick gains sets the steady-state roll rate and sideslip commands. Analogous to the longitudinal control laws, the pre-filters act as the command models which define the desired aircraft response dynamics, and are given by:

$$\frac{p_{cm}}{\delta_{lat_s}} = \frac{K_{lat}}{\tau_{p_{cm}} s + 1} \quad (6)$$

in the lateral axis, and:

$$\frac{\beta_{cm}}{\delta_{ped_s}} = \frac{K_{ped}\omega_{b_{cm}}^2}{s^2 + 2\zeta_{b_{cm}}\omega_{b_{cm}}s + \omega_{b_{cm}}^2} \quad (7)$$

in the directional axis. Where,

- K_{lat} sets the desired steady state roll rate,
- K_{ped} sets the desired steady state sideslip,
- $\tau_{p_{cm}}$ is set equal to the bare-airframe roll mode time constant τ_r ,
- $\zeta_{b_{cm}}$ is set to 0.7 to provide a well damped directional response, and
- $\omega_{b_{cm}}$ is set to the bare-airframe Dutch roll frequency ω_{dr} to retain the good inherent Dutch roll frequency of the bare-airframe aerodynamic design and to not overdrive the actuators.

Note that the bare-airframe roll mode time constant and Dutch roll frequency values in the command models are selected for the nominal weight/CG configuration (Figure 3, Nominal Design Point) at each flight condition. Crossfeed gains in the feed-forward path (K_{xfeed} , Figure 11) are used to achieve converse off-axis responses.

The feedback path in the lateral/directional axis (shown in Figure 12) is comprised of proportional and integral roll rate error paths fed back to the aileron, proportional, derivative, and integral sideslip error paths fed back to the rudder, and crossfeed paths used to eliminate contributions of the off-axis responses in the on-axis responses.⁹

At each of the 92 flight condition design points (Figure 2), the feedback gains were optimized to meet 31 Tier 1 specifications listed in Table 2. The table also provides the eight Tier 2 specifications used as a check at the end of the optimization. As in the longitudinal axis, control law performance robustness to changes in weight/CG was provided by enforcing a minimum crossover frequency ($\omega_c = 3.5$ rad/sec) for both the lateral axis (loop broken at the aileron actuator command) and the directional axis (loop broken at the rudder actuator command). In addition, key specifications (stability and Nichols margins and model following performance) were enforced for the Light and Heavy design points (Figure 3) as well as the Nominal design point. This resulted in a smooth gain schedule with predicted Level 1 handling qualities for the full range of flight conditions and loading configurations.

Figure 13 and Figure 14 show the optimization results for one of the 92 design points—the 250 kts (KCAS), 15,000 ft, flaps up flight condition. As was the case for the longitudinal results presented above, all Tier 1 specifications are met within the design procedure. Several of the specifications are on the boundary, which is the Pareto optimal solution.

Figure 15 shows the commanded roll rate p_{cm} frequency response, as well as the aircraft roll rate p response, for the nominal loading configuration. Figure 16 shows the commanded sideslip β_{cm} frequency response, as well as the aircraft sideslip β response, for the nominal loading configuration. Both roll rate and sideslip responses match their respective commanded responses well over a wide frequency range, indicating excellent command model following performance in both axes.

Figure 17 shows the broken-loop frequency responses BL_p , for the loop broken at the aileron actuator, and Figure 18 shows the broken-loop frequency responses BL_β , for the loop broken at the rudder actuator. The design is on the minimum crossover frequency requirements ($\omega_{c_p} = 3.5$ rad/sec and $\omega_{c_\beta} = 3.5$ rad/sec) in both axes, with sufficient stability margins.

Figure 19 shows a 1 sec piloted lateral stick pulse response. The closed-loop aircraft exhibits a first-order roll response, with no overshoot or oscillations, which is expected for the first-order command model used in the lateral axis. The sideslip response is small, and meets the sideslip excursion specification (MIL-STD-1797B⁶) and the turn coordination specification (SAE-AS94900²¹).

Figure 20 shows the lateral acceleration response to a 1-cosine sideslip gust. The figure shows that the second peak of the lateral acceleration response is smaller in magnitude than the first, which is the load alleviation goal enforced by the sideslip gust specification.

As in the longitudinal axis, similar lateral/directional results were generated for the remaining 91 design points, which resulted in a smooth gain schedule with predicted Level 1 handling qualities for the full range of flight and loading configurations.

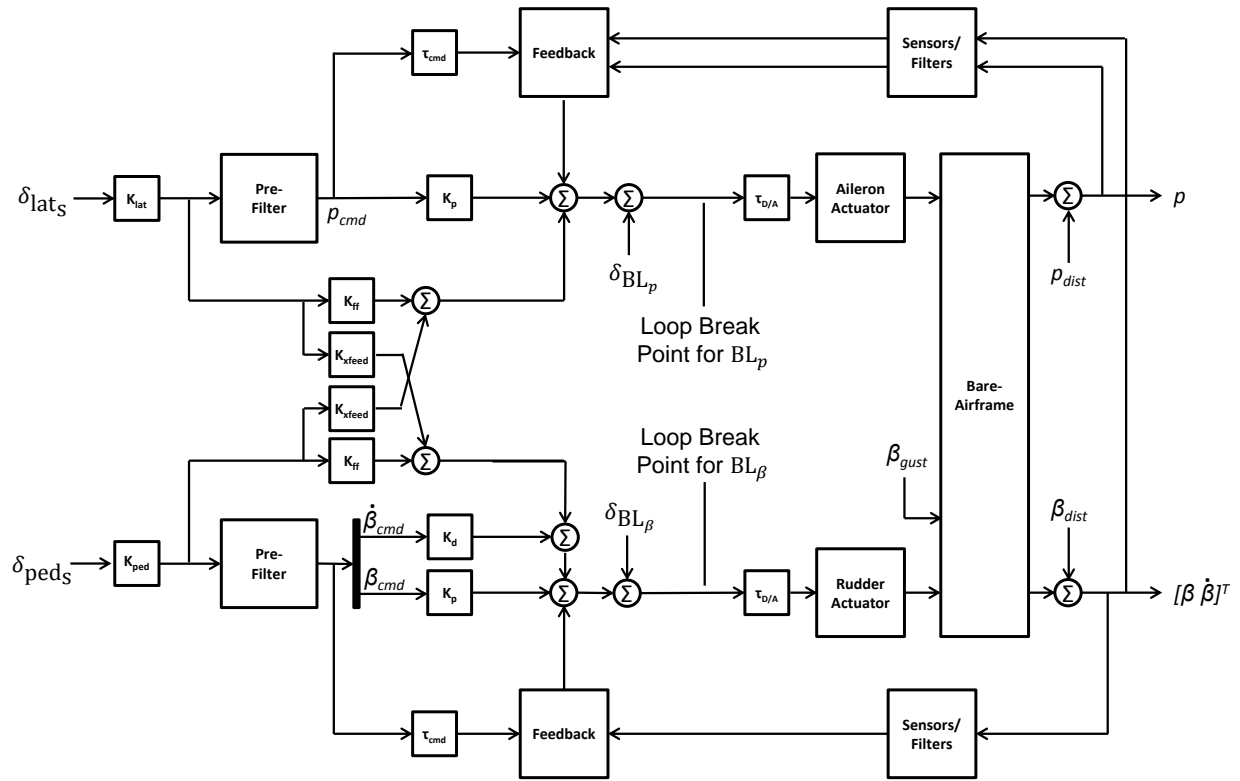


Figure 11. Schematic of lateral/directional control law block diagram.

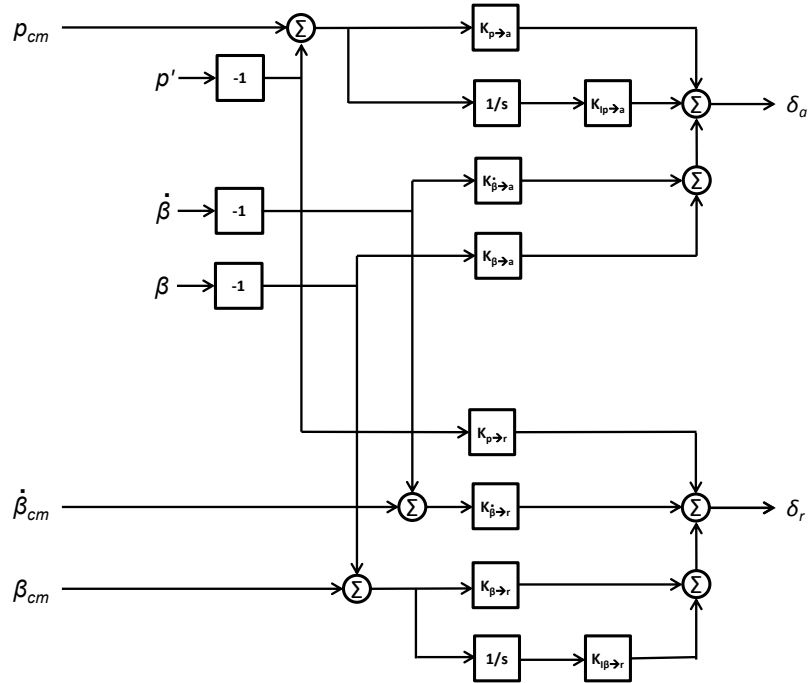


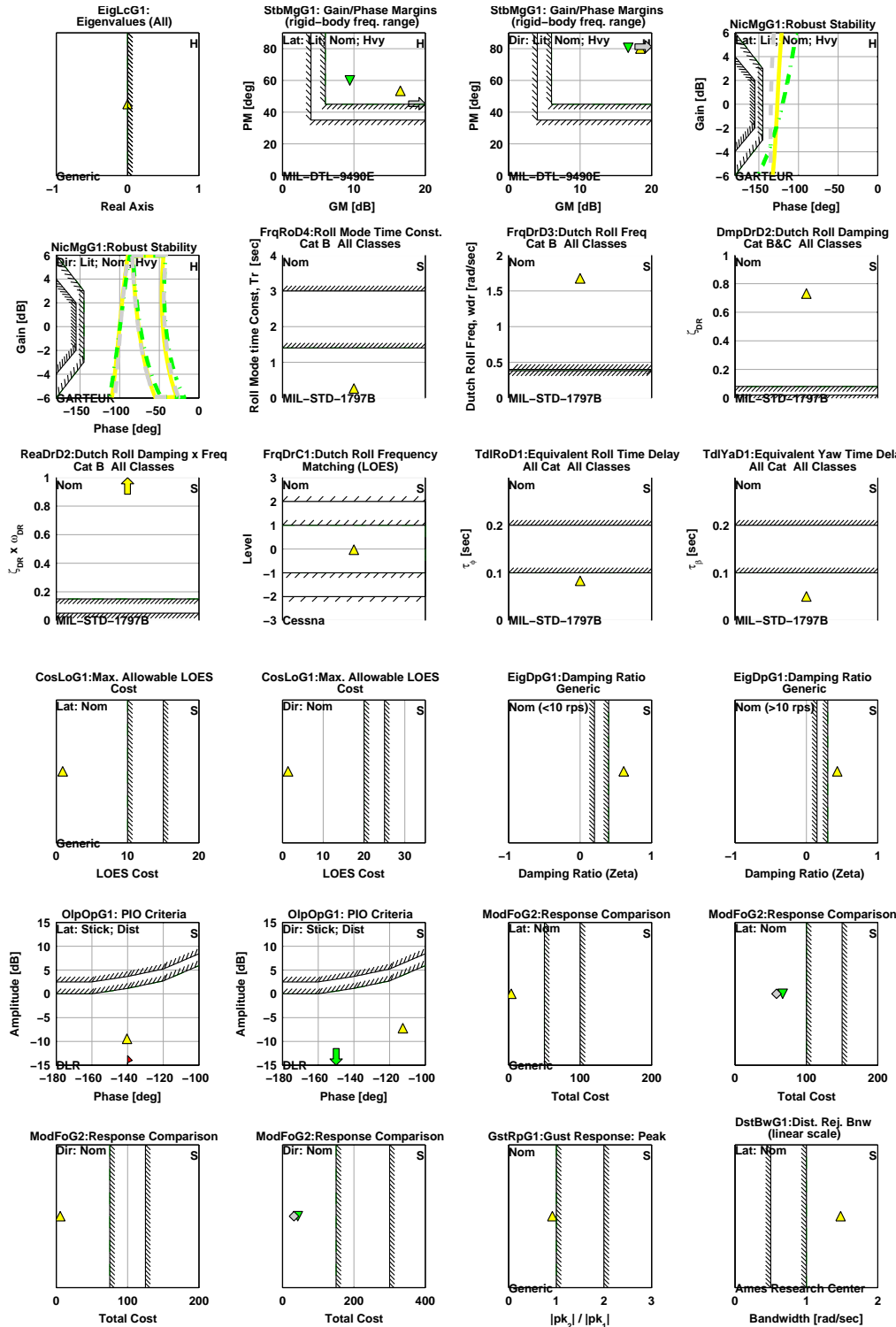
Figure 12. Schematic of lateral/directional control law feedback block.

Table 2. Lateral/Directional Optimization Specifications

Constraint	Spec Name	Description (Motivation)	Domain*	Source	Config.†
<i>Tier 1</i>					
Hard	EigLcG1	Eigenevalues in L.H.P. (Stability)	S	Generic	N
	StbMgG1	Gain and phase margins loop broken at aileron actuator (Stability)	F	MIL-DLT-9490E	L,N,H
	StbMgG1	Gain and phase margins loop broken at rudder actuator (Stability)	F	MIL-DLT-9490E	L,N,H
	NicMgG1	Nichols Margins loop broken at aileron actuator (Stability)	F	GARTEUR	L,N,H
	NicMgG1	Nichols Margins loop broken at rudder actuator (Stability)	F	GARTEUR	L,N,H
Soft	FrqRoD4	Roll model time constant (HQ)	L	MIL-STD-1797B	N
	FrqDrD3	Dutch roll frequency (ω_{dr}) (HQ)	L	MIL-STD-1797B	N
	DmpDrD2	Dutch roll damping (ζ_{dr}) (HQ)	L	MIL-STD-1797B	N
	ReaDrD2	$\zeta_{dr}\omega_{dr}$ (HQ)	L	MIL-STD-1797B	N
	FrqDrC1	$\omega_{dr} \pm 20\%$ open-loop (HQ, Act. Activity)	L	Generic	N
	TdlRoD1	Roll axis equivalent time delay (HQ)	L	MIL-STD-1797B	-
	TdlYaD1	Yaw axis equivalent time delay (HQ)	L	MIL-STD-1797B	-
	CosLoG1	Max roll rate LOES Cost (HQ)	L	Generic	N
	CosLoG1	Max sideslip LOES Cost (HQ)	L	Generic	N
	EigDpG1	Eigenvalue Damping (HQ, Loads)	S	Generic	N
	OlpOpG1	Aileron/rudder actuator Open Loop Onset Point for pilot input (PIO)	F	DLR	N
	OlpOpG1	Aileron/rudder actuator Open Loop Onset Point for disturbance input (PIO)	F	DLR	N
	ModFoG2	Lateral axis command model following cost (HQ)	F	Generic	L,N,H
	ModFoG2	Directional axis command model following cost (HQ)	F	Generic	L,N,H
	GstRpG1	Sideslip gust response (Loads)	T	Generic	N
	DstBwG1	Roll attitude disturbance rejection bandwidth (Loads, Ride Quality)	F	ADS-33E	N
	DstBwG1	Sideslip disturbance rejection bandwidth (Loads, Ride Quality)	F	ADS-33E	N
	DstPkG1	Roll attitude disturbance rejection peak (Loads, Ride Quality)	F	ADS-33E	N
	DstPkG1	Sideslip disturbance rejection peak (Loads, Ride Quality)	F	ADS-33E	N
	MaxMgT1	Maximum tail loads during rudder kick, gust, and turbulence (Loads)	T	Generic	N
	CrsMnG1	Minimum $\omega_c \geq 3.5$ rad/sec, loop broken at aileron actuator (Robustness)	F	Generic	N
	CrsMnG1	Minimum $\omega_c \geq 3.5$ rad/sec, loop broken at rudder actuator (Robustness)	F	Generic	N
	Summed	CrsLnG1	Minimize crossover frequency, loop broken at aileron actuator (Act. Activity)	F	Generic
CrsLnG1		Minimize crossover frequency, loop broken at rudder actuator (Act. Activity)	F	Generic	N
Obj.	RmsAcG1	Minimize aileron actuator RMS (Act. Activity)	F	Generic	N
	RmsAcG1	Minimize rudder actuator RMS (Act. Activity)	F	Generic	N
<i>Tier 2</i>					
Check Only	OscRoD4	Roll oscillations (HQ)	T	MIL-STD-1797B	-
	CouRsD2	Sideslip excursion (HQ)	T	MIL-STD-1797B	-
	PioRoD1	Roll PIO criteria (HQ)	T	MIL-STD-1797B	-
	TrnCrD2	Turn coordination (HQ)	T	SAE-AS94900	-
	OscRoD7	Roll rate transfer function zero cancellation	S	Generic	-
	InnRoD1	Innocenti lateral tracking	F	Innocenti	-
	BnwRoD1	Roll attitude bandwidth, phase delay	F	WL-TR-94-3162	-
	NicMgG1	Nichols Margins loop broken at sensors (Stability)	F	GARTEUR	-

*F = Frequency domain specification, T = Time domain specification, L = LOES specification, S = s-plane

†N = Nominal weight/CG configuration only, L,N,H = Light, Nominal, and Heavy weight/CG configurations



Problem Name: CJ1_Cruise_Lateral/Directional

Iteration: 0

Page 1

Print Time: 06-Dec-2016, 10:15

Figure 13. Handling qualities specification results of the optimized design (1/2) (lateral/directional axis, 250 kts, 15,000 ft flight condition).

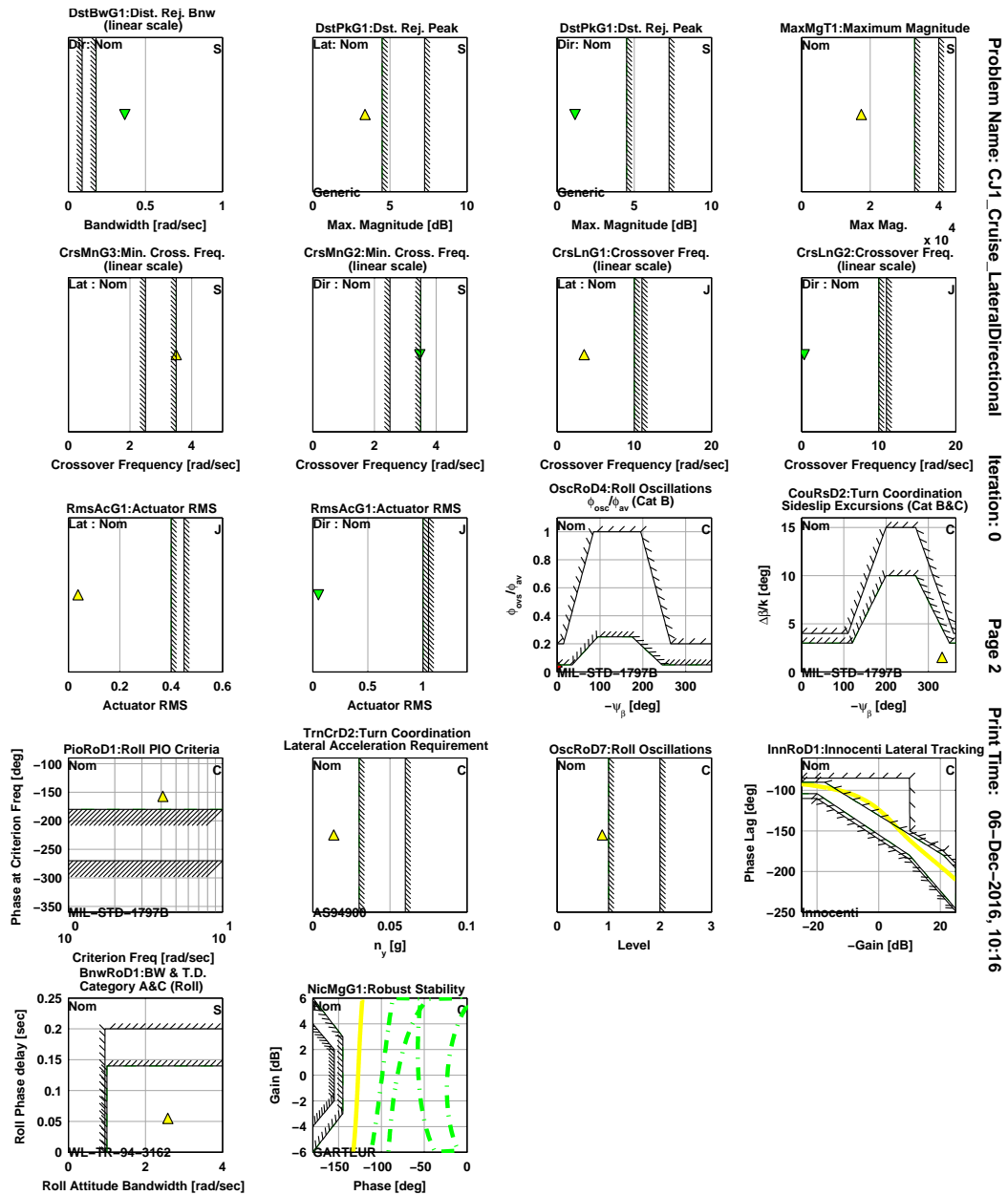


Figure 14. Handling qualities specification results of the optimized design (2/2) (lateral/directional axis, 250 kts, 15,000 ft flight condition).

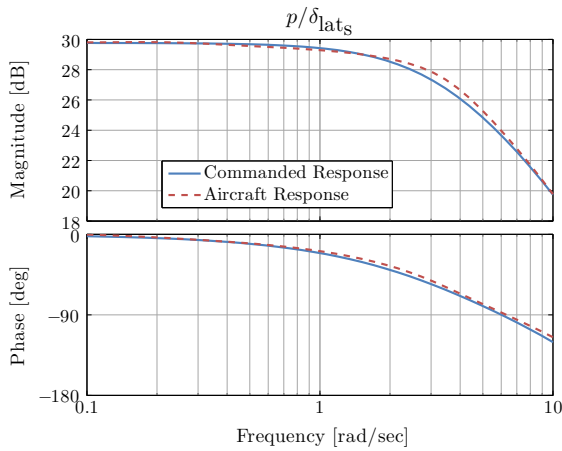


Figure 15. Roll rate frequency response (250 kts, 15,000 ft flight condition; Nominal loading configuration).

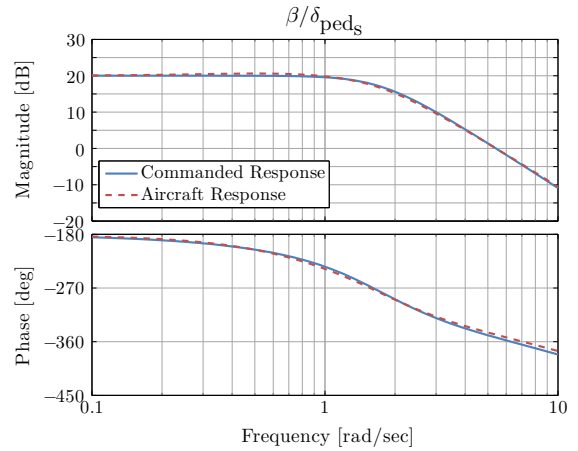


Figure 16. Sideslip frequency response (250 kts, 15,000 ft flight condition; Nominal loading configuration).

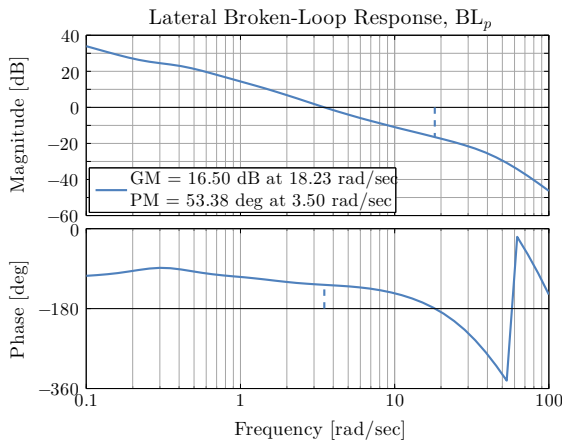


Figure 17. Lateral broken-loop (at input to aileron actuator) frequency response (250 kts, 15,000 ft flight condition; Nominal loading configuration).

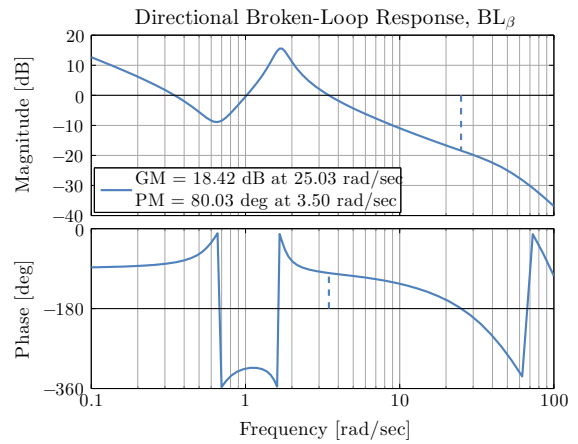


Figure 18. Directional broken-loop (at input to rudder actuator) frequency response (250 kts, 15,000 ft flight condition; Nominal loading configuration).

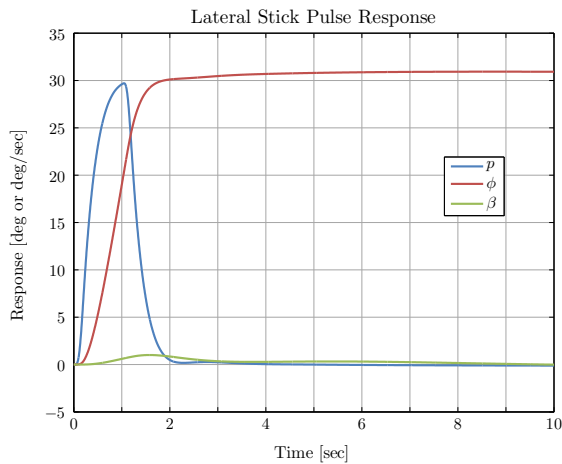


Figure 19. Lateral stick 1 sec pulse response (250 kts, 15,000 ft flight condition; Nominal loading configuration).

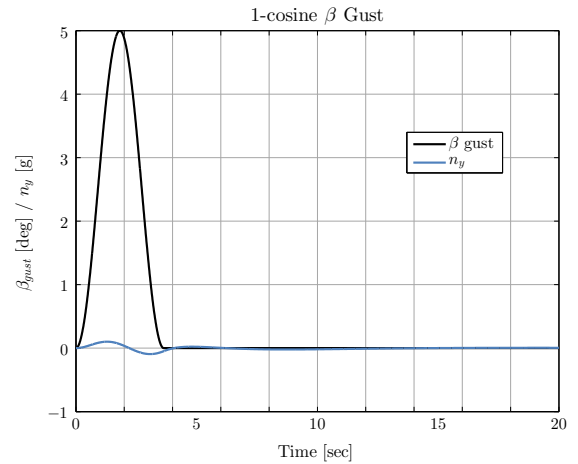


Figure 20. 1-cos sideslip gust response (250 kts, 15,000 ft flight condition; Nominal loading configuration).

C. Gain Schedule Implementation

A smooth gain schedule was provided by CONDUIT[®] optimization (as described in Sections III.A and III.B), and was implemented in a 3D lookup table for each gain, as a function of Mach, dynamic pressure, and flap deflection. Figures 21 and 22 show the flaps up gain schedules for one of the longitudinal axis feedback gains and one of the lateral axis feedback gains, respectively. Note that some points outside the flight envelope were extrapolated from the optimized designs to provide the lookup tables with rectangular grids. The points are connected to show the linear interpolation scheme used by the lookup table. As the figures show, the curves are smooth and did not require any additional smoothing or spline fitting.

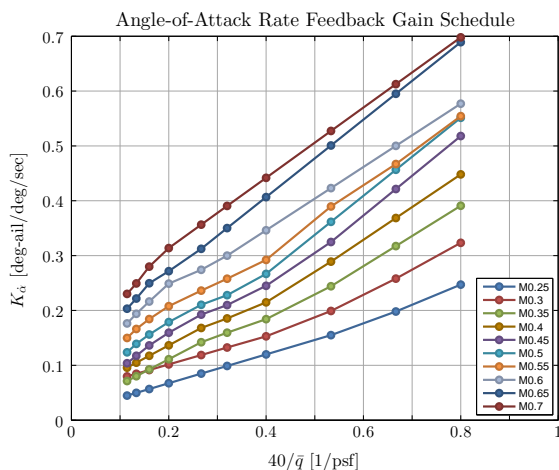


Figure 21. Example longitudinal feedback gain schedule.

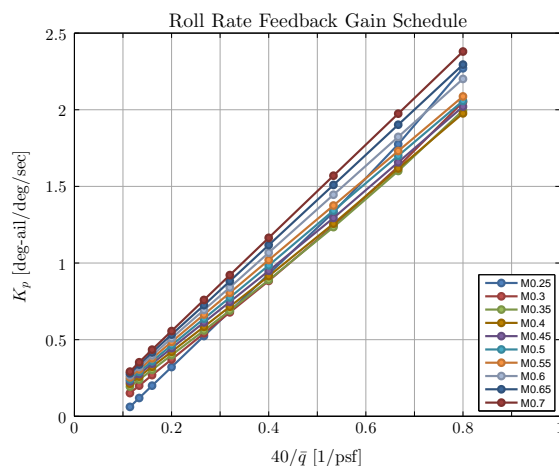


Figure 22. Example lateral/directional feedback gain schedule.

D. Stick Characteristics

The VSS LJ-25 is equipped with a center stick for the evaluation pilot. The FBW control law inputs (δ_{lon_s} in Figure 4 and δ_{lat_s} and δ_{ped_s} in Figure 11) were stick positions. Table 3 lists the stick and pedal force feel system characteristics that were used during all evaluations.

Table 3. Force Feel System Characteristics

	Pitch Stick	Roll Stick	Pedals
Gradient [lb/in]	6	3.5	40
Preload [lb]	0.75	0	0
Damping Ratio [-]	0.7	0.7	0.7
Frequency [rad/sec]	16	16	16
Deflection (δ) Range [in]	4.1	5.3	3.2
Force (F) Range [lbs]	25.0	19.0	130.0

E. Modifications Based on Initial Flight Testing

As described in Section III.B, at each design point (flight condition) the lateral axis command-model time constant ($\tau_{p_{cm}}$ in Equation 6) was set to the bare-airframe roll mode time constant τ_r of a center-of-the-envelope loading configuration (Nominal Design Point, Figure 3). This time constant was initially selected to avoid over-driving the actuators, while still meeting all Level 1 handling qualities requirements from MIL-STD-1797B. However, pilots commented during initial flight tests that the roll rate response was too slow. Based on the pilot feedback, the command-model time constant was set instead to the bare-airframe roll mode time constant of the light loading configuration (Light Design Point, Figure 3) which has empty

tip tanks—a more typical configuration for other transport aircraft. This resulted in a faster command-model time constant and a faster speed of response, at the cost of additional actuator usage in some loading configurations.

Figure 23 shows the lower-order equivalent system (LOES) roll mode time constant τ_{r_e} of the closed-loop system for all flight conditions and loading configurations as a function of inverse dynamic pressure ($40/\bar{q}$). The figure shows the results for both the original gain schedule and the updated gain schedule with the reduced lateral axis command-model time constant. On average, the equivalent roll mode time constants τ_{r_e} of the updated gain schedule were about 50% those of the original gain schedule. The solid Level boundaries plotted on the figure are from MIL-STD-1797B⁶ for Category B (gradual maneuvers) flight phase and All Classes of aircraft (the specification boundaries used in the control law optimization). These also correspond to the Category A (rapid maneuvers) flight phase boundaries for Class II and III aircraft (of which the Learjet is one).

Both the original and the updated gain schedules meet the Category B and Category A, Class II and III boundaries. The updated gain schedule, which received better HQRs, meets the Category A, Class I (small, light aircraft) and VI (highly maneuverable aircraft) boundaries for all but two low-speed configurations, suggesting that these boundaries may be more applicable.

Figure 24 shows the roll attitude bandwidth values of the original and updated gain schedules and specification boundaries.⁴ The specification applies to Category A and C flight phases,⁴ and was a Tier 2 specification that was not used directly in the control law optimization, but only as a check afterward. The updated gain schedule meets the Level 1 bandwidth and phase delay requirements for all but one low-speed flight condition. This suggests that this specification should be included as a Tier 1 requirement, enforced during the control law optimization, even for a Category B design such as this one.

Pilots commented positively about the speed of response in the longitudinal axis in the initial testing, and so the longitudinal command-model frequency (ω_{cm} in Equation 1) was not updated.

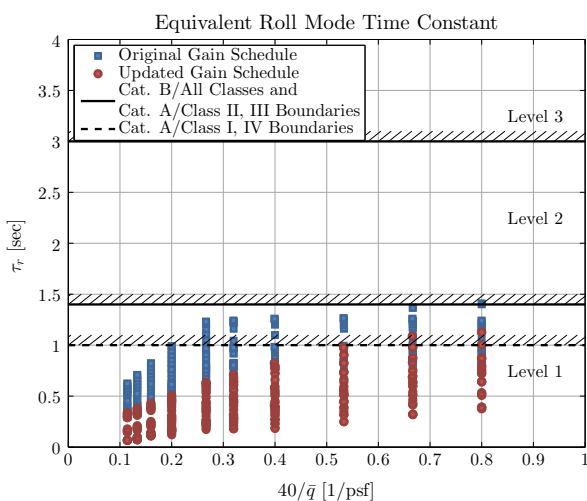


Figure 23. Equivalent roll mode time constant values and MIL-STD-1797B specification boundaries (All flight conditions; All loading configurations).

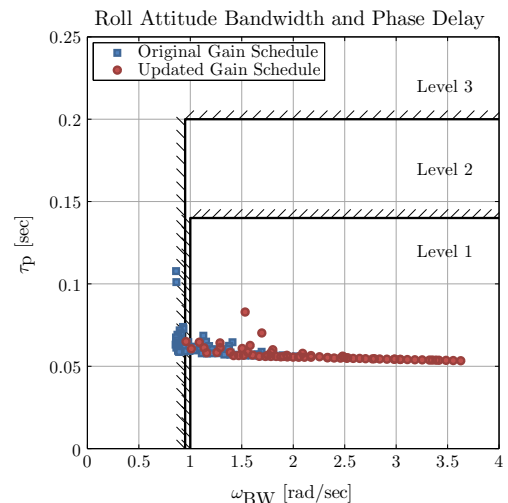


Figure 24. Roll attitude bandwidth and phase delay values and MIL-STD-1797B specification boundaries (All flight conditions; All loading configurations).

In addition to the faster lateral axis command-model time constant, both the longitudinal and lateral stick gains (K_{lon} in Figure 4 and K_{lat} in Figure 11) which determine the steady-state normal acceleration and roll rate commands per stick deflection, were increased based on the initial evaluation. The gains were scaled to match more closely the stick gains of the open-loops baseline VSS configuration.¹⁴ Figure 25 shows the normal acceleration frequency response for the baseline VSS (open-loop) Learjet and the closed-loop system with the original and updated stick gains, for the 250 kts, 15,000 ft flight condition. Note that the frequency responses are shown for stick force F_{lon_s} as the input, to assess the stick force per g gradient between the configurations. At this flight condition, the baseline VSS Learjet has a stick force per g gradient of $dF_{lon_s}/dn_z = 6.75$ lbs/g. The control laws with the original stick gain provide a stick force per g gradient of $dF_{lon_s}/dn_z = 29.45$ lbs/g, which meets the FAR requirements,²⁰ but is over four times the baseline VSS.

The control laws with the updated stick gain provide a stick force per g gradient of $dF_{lon_s}/dn_z = 9.82$ lbs/g, closer to the baseline VSS value.

Figure 26 shows the roll rate frequency response for the baseline VSS Learjet and the closed-loop system with the original and updated stick gains, for the 250 kts, 15,000 ft flight condition. As in the normal acceleration responses, the roll rate frequency responses here are shown for stick force F_{lat_s} as the input. At this flight condition, the baseline VSS Learjet has a stick force per steady state roll rate gradient of $dF_{lat_s}/dp = 0.133$ lbs/deg/sec. The control laws with the original stick gain provide a stick force per steady state roll rate gradient of $dF_{lat_s}/dp = 0.477$ lbs/deg/sec, while the control laws with the updated stick gain provide a stick force per steady state roll rate gradient of $dF_{lat_s}/dp = 0.239$ lbs/deg/sec. Making the control law and baseline VSS stick gradients more similar was important for back-to-back comparisons of the FBW control laws and the baseline VSS Learjet to ensure stick gradients did not drive the differences.

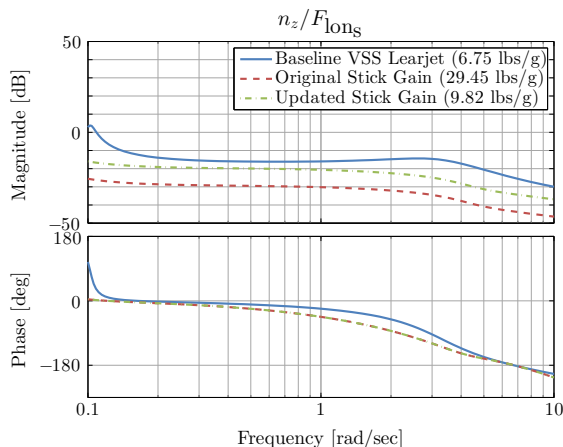


Figure 25. Closed-loop normal acceleration response (250 kts, 15,000 ft; Nominal loading configuration).

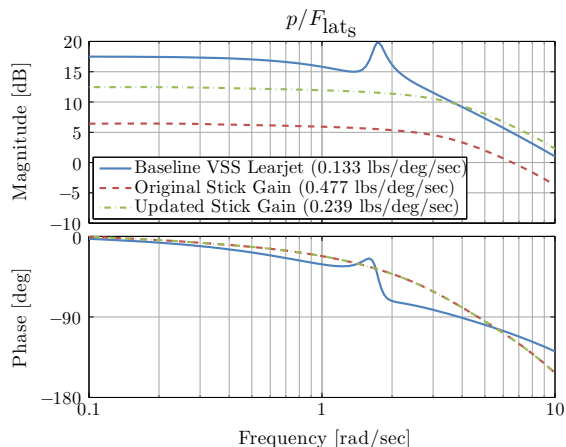


Figure 26. Longitudinal broken loop response (250 kts, 15,000 ft; Nominal loading configuration).

IV. Flight Test Description and Results

The flight test campaign consisted of two preliminary and one formal evaluations of the control laws, all taking place at the USAF Test Pilot School (TPS), Edwards Air Force Base (AFB), CA. The first evaluation was done as part of a USAF TPS Test Management Program,²² and two TPS students evaluated the control laws. The second evaluation was completed by three Textron Aviation Senior Experimental Test Pilots with an average of 3300 hours of jet time. Finally, the formal evaluation was performed by two TPS instructor pilots (IPs), who have over 5000 and 1850 flight hours, respectively.

Each evaluation consisted of multiple sorties, with each pilot getting to fly the majority of the evaluation tasks. The following sections will describe the model validation and handling qualities tasks flown and results. Ref. 22 provides additional results not presented here, from the first flight test evaluation, covering a flying qualities analysis and validation of the control laws.

A. Model Validation

In order to validate the implementation of the control laws on the VSS, dynamic checks were performed at two flight conditions—cruise (250 kts, 15,000 ft) and powered approach (185 kts, 15,000 ft, flaps 20, gear down). This was done by conducting both piloted closed-loop (δ_{lon_s} , Figure 4; δ_{lat_s} and δ_{ped_s} , Figure 11) and automated broken-loop ($\delta_{BL_{n_z}}$, Figure 4; δ_{BL_p} and δ_{BL_β} , Figure 11) frequency sweeps. The frequency sweep flight data were analyzed using CIFER^{®23} to extract the appropriate frequency responses and compare to those of the linear point models used in the control law development. Two responses were analyzed in each axis: the closed-loop piloted response comparison to validate the implementation of the feed-forward and feedback sections of the control laws and the broken-loop response comparison to validate the implementation of the feedback section of the control laws.

Figures 27 and 28 show the cruise configuration closed-loop n_z/δ_{lon_s} and broken-loop (at the elevator actuator command) BL_{n_z} frequency responses in the longitudinal axis for both the flight data and analysis model. The figures show a nearly perfect agreement between the flight data and analysis model, validating both the bare-airframe stitched model used for the control law optimization and the implementation of the longitudinal control laws and gain schedule in the VSS. An unmodeled tip tank fuel slosh mode can be seen as a notch in the normal acceleration flight data frequency response (solid blue line, Figure 27) at around $\omega = 20$ rad/sec. This mode only shows up when the tip tanks are near-full, and is not present in the powered approach normal acceleration flight data frequency response (Figure 33).

Figures 29 and 30 show the cruise configuration closed-loop p/δ_{lat_s} and broken-loop (at the aileron actuator command) BL_p frequency responses in the lateral axis for both the flight data and analysis model. Figures 31 and 32 show the cruise configuration closed-loop β/δ_{ped_s} and broken-loop (at the rudder actuator command) BL_β frequency responses in the directional axis for both the flight data and analysis model. As with the longitudinal axis, the figures here show an excellent agreement between the flight data and model, validating the bare-airframe stitched model and implementation of the lateral/directional control laws and gain schedule in the VSS.

Finally, Figures 33 and 34 show the powered approach configuration longitudinal axis closed-loop n_z/δ_{lon_s} and broken-loop BL_{n_z} frequency responses for both the flight data and analysis model. There is an excellent agreement between flight data and the analysis model in the powered approach configuration, suggesting proper implementation of the gain schedule and validating the bare-airframe model used in the control law optimization. Excellent agreement between the flight data and analysis model was seen in the lateral and directional axes for the power approach configuration as well.

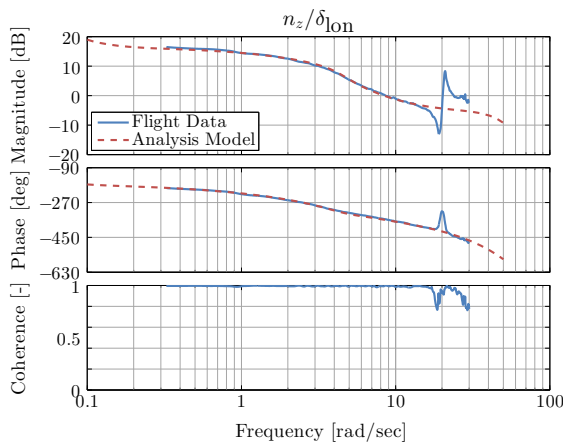


Figure 27. Closed-loop normal acceleration response (250 kts, 15,000 ft).

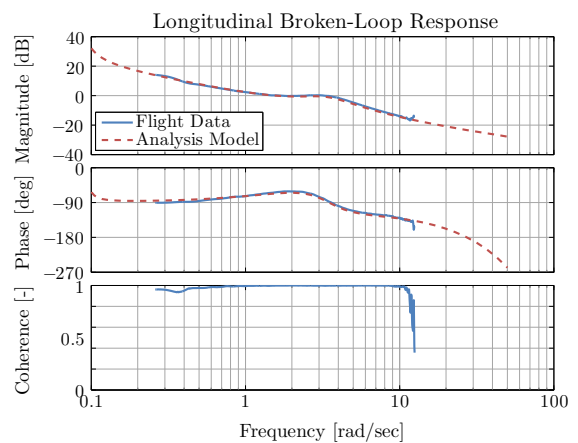


Figure 28. Longitudinal broken loop response (250 kts, 15,000 ft).

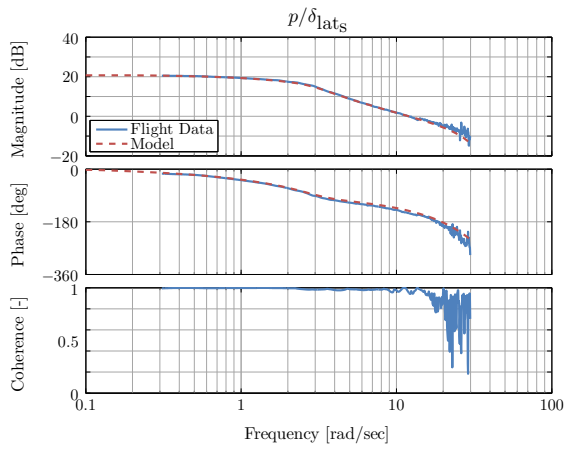


Figure 29. Closed-loop roll rate response (250 kts, 15,000 ft).

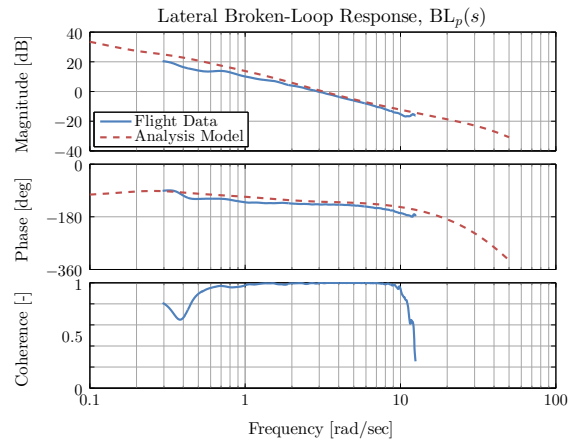


Figure 30. Lateral broken loop response (250 kts, 15,000 ft).

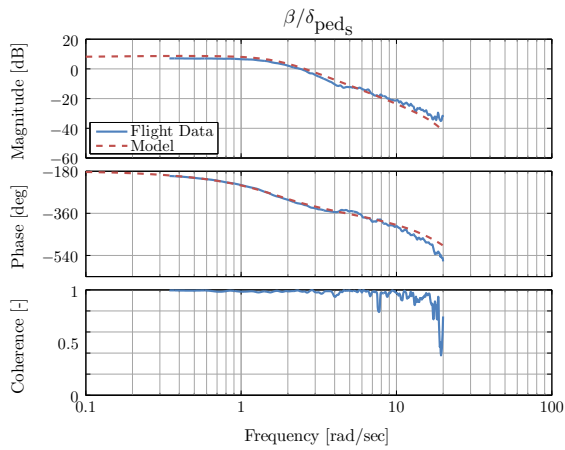


Figure 31. Closed-loop sideslip response to pedal input (250 kts, 15,000 ft).

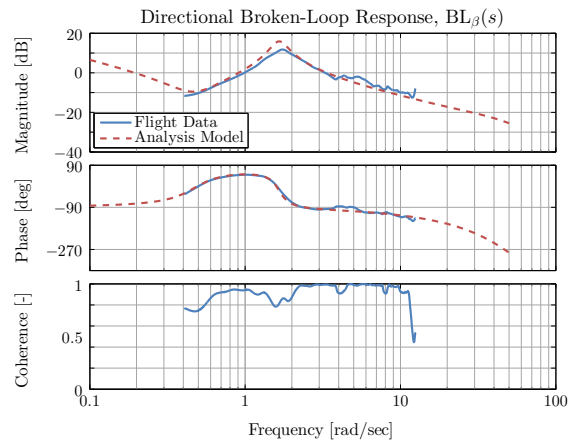


Figure 32. Directional broken loop response (250 kts, 15,000 ft).

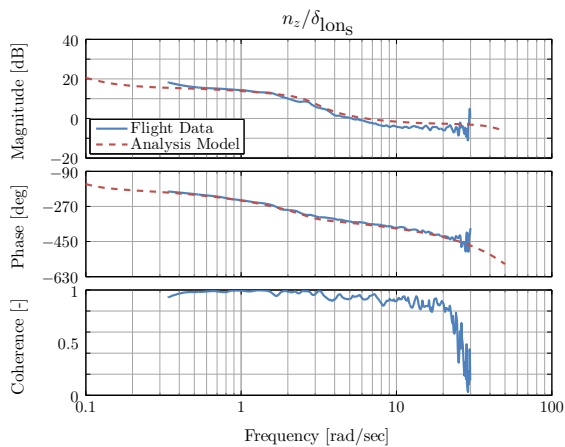


Figure 33. Closed-loop normal acceleration response (185 kts, 15,000 ft, flaps 20, gear down).

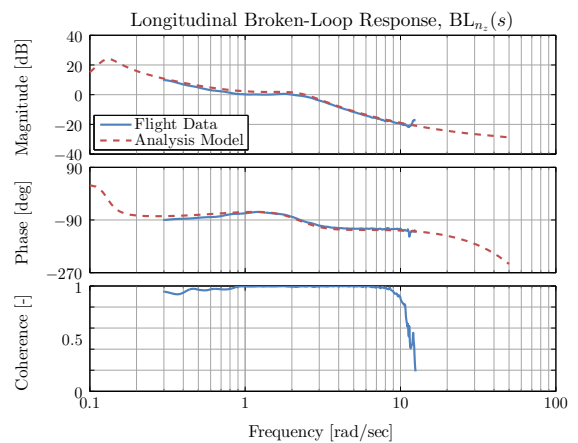


Figure 34. Longitudinal broken loop response (185 kts, 15,000 ft, flaps 20, gear down).

B. Handling Qualities Evaluation

Handling qualities tasks were completed both at altitude and during approach and landing phases of flight. The following sections describe the tasks and results in more detail.

1. Pitch and Bank Angle Capture

Pitch and bank angle capture tasks were used to evaluate the handling qualities for gross acquisition. As stated in MIL-STD-1797B,⁶ these tasks are usually done “almost precognitively by the pilot” and are “usually over so quickly that they do not lend themselves well to use with the [Cooper-Harper HQR] scale.” Therefore, desired and adequate performance bounds were not used for these tasks. Instead, pilots were asked to acquire the target attitudes as closely as possible and at a rate they would find aggressive for a business jet, and then to provide comments.

The Textron Aviation test pilots flew *back-to-back* pitch and bank angle captures in the Learjet with the control laws engaged and in an open-loop direct (baseline VSS) mode in order to assess the HQ improvement of the advanced FBW ($n_z u, p-\beta$) control laws. The pilots reported that it was “easy to hit [the] target” with the advanced FBW control laws engaged. For the open-loop mode, pilots commented that the roll axis “felt much looser” and required “several small inputs to capture and maintain bank angle after initially stopping the roll.” This was not the case when the advanced FBW control laws were engaged. These comments are consistent with the increased overall damping of the control laws over the bare-airframe.

Pitch and bank angle captures were also flown by the USAF TPS IPs in their formal evaluations. They commented that with the advanced FBW control laws active, the aircraft “stops without overshoot” during pitch captures and that they could be “aggressive.” In roll, the pilots commented that with the control laws active, they did not need to “hunt” for the target attitude and that the aircraft “sticks where you put it.”

2. Discrete Tracking

The discrete tracking task is based on the methodology of MIL-STD-1797B,⁶ and was used to evaluate a combination of gross acquisition and fine tracking in a high pilot-gain task. A target symbol was displayed on the VSS Head Down Display (HDD) which commanded simultaneous pitch and roll changes that the evaluation pilot was instructed to follow. The pitch and roll commands were composed of steps and ramps, as illustrated for an example record in Figure 35. This version of the tracking task is well-suited to business jets, where a pilot will make a discrete correction in a flight parameter (e.g., attitude, flight-path angle, airspeed, etc.) and attempt to hold the new value for a period of time.

Task performance criteria are shown in Table 4. Individual pitch and roll scores were provided, in addition to a combined score (defined as percent time spent within both the pitch and roll desired and adequate bounds). Overall handling qualities performance was rated on the Cooper-Harper Handling Qualities Rating (HQR) scale²⁴ based on the ability to achieve a combined desired or adequate task performance.

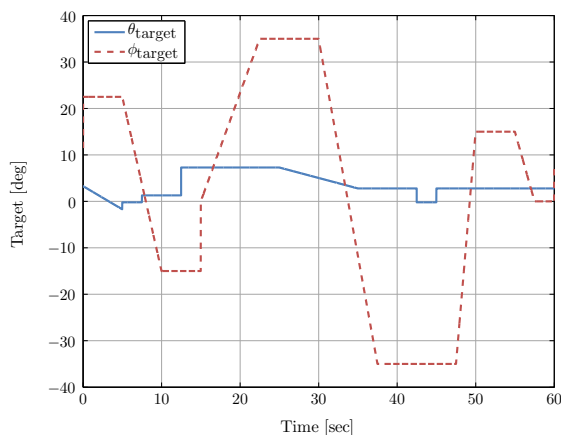


Figure 35. Example discrete tracking sequence.

Table 4. Performance Criteria - Tracking

	Desired	Adequate
<i>Pitch</i>		
Remain within ± 0.5 deg for X percent of the time	50%	-
Remain within ± 1.0 deg for X percent of the time	-	50%
No PIO	✓	✓
<i>Roll</i>		
Remain within ± 5.0 deg for X percent of the time	50%	-
Remain within ± 10.0 deg for X percent of the time	-	50%
No PIO	✓	✓

The discrete tracking task results shown here were flown by the two USAF TPS IPs. For this task, all evaluations were flown only with the advanced FBW control laws active (no open-loop evaluations), at two flight conditions:

1. 150 kts, 10,000 ft, powered approach configuration (flaps 20, gear down)
2. 250 kts, 15,000 ft, cruise configuration

Figure 36 shows the performance attained during the tasks at each flight condition for each pilot. Performance is shown in terms of percent time spent within the desired bounds (Table 4), and is shown for the pitch axis, roll axis, and combined. The points on Figure 36 are the average performance for all of a pilot’s data runs, while the error bars show the best and worst performance.

For the discrete tracking task, which both pilots agreed is a *well-suited task to assess business jet control laws*, the pilots were able to attain Level 1 performance with the advanced FBW control laws in both flight conditions tested. This demonstrates the consistent performance of the gain schedule across the flight envelope. Furthermore, the pilots provided Level 1 HQRs for this task, as shown in Figure 37.

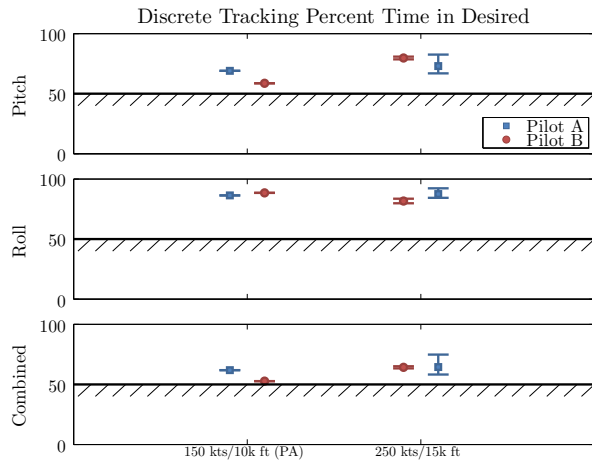


Figure 36. Discrete tracking task performance.

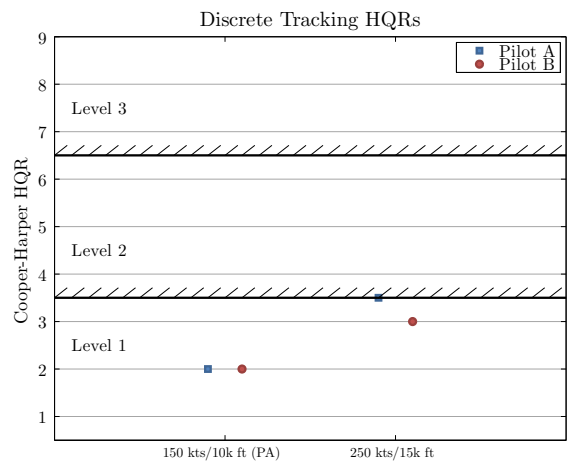


Figure 37. Discrete tracking HQRs.

3. Sum-of-Sines Tracking

The sum-of-sines tracking task was used primarily to look for handling qualities “cliffs” or PIO tendencies in the advanced FBW control laws by evaluating continuous closed-loop controllability in a high pilot-gain task. This task is based on the methodology of the Air Force Handling Qualities Demonstration Maneuver Catalog.¹²

For this task, the pitch and roll commands displayed on the HDD were generated using a randomized sum-of-sines, as illustrated for an example record in Figure 38. The record starts with a 5 sec ramp-in and

settle time, followed by the 50 sec scoring time, and ending with a 5 sec ramp-out time. The phasing of the sine waves was randomized for each run to make sure the pilots saw a different signal each time.

Figure 39 shows the power spectral density of the target signals. The signal cutoff frequency²³ ω_{co} is defined as the half-power frequency of the target signal and is a good measure of the target signal bandwidth. This, therefore, also approximates the task bandwidth. The cutoff frequency is about $\omega_{co} = 0.7$ rad/sec in both axes. The signal RMS values are about 1 deg in pitch and 7 deg in roll. Desired and adequate performance criteria are the same as for the discrete tracking task, shown in Table 4.

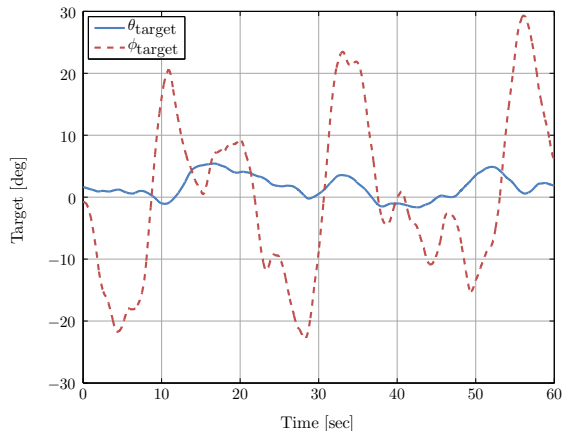


Figure 38. Example sum-of-sines tracking sequence.

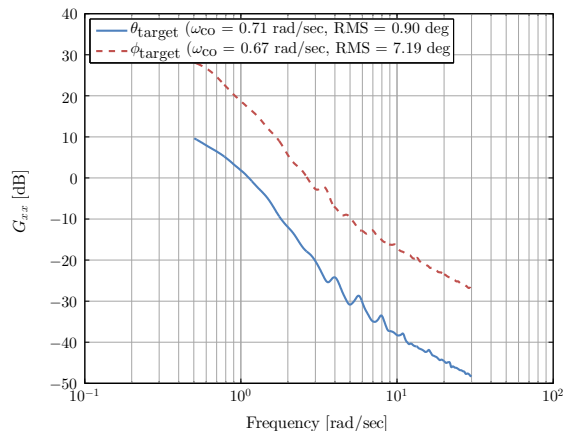


Figure 39. Sum-of-sines tracking sequence power spectral density.

The sum-of-sines tracking task results shown here were flown by the two USAF TPS IPs. All sum-of-sines tracking evaluations were flown only with the advanced FBW control laws active at several flight conditions (and loading configurations due to fuel burn throughout the flight):

1. 150 kts, 10,000 ft, powered approach configuration (flaps 20, gear down)
2. 185 kts, 15,000 ft, cruise configuration
3. 250 kts, 15,000 ft, cruise configuration
4. 300 kts, 15,000 ft, cruise configuration

Figure 40 shows the performance attained during the tasks at each flight condition for each pilot. Performance is shown as percent of time spent within the desired bounds, with the combined value being percent of time spent within both the pitch and roll desired bounds. The points on Figure 40 are the average performance for all of a pilot’s data runs, while the error bars show the best and worst performance. Figure 41 shows the assigned pilot HQRs for the sum-of-sines tracking task.

The results of the sum-of-sines tracking task are consistent with those attained during a previous simulation testing of these control laws.¹⁰ First, very similar performance was attained for the different flight conditions and loading configurations tested, showing good robustness of the control laws to changes in aircraft loading and consistent performance of the gain schedule across the flight envelope. Second, pitch performance was in the 45–60% range while roll performance was in the 65–85% range. The combined performance was in the 35–50% range, and was used by the pilots to form their ratings. Since in general desired performance was not attained in the sum-of-sines tracking task, pilot ratings were Level 2 (HQR 4 and HQR 5). Pilot A was able to attain desired performance on the final run, at the 300 kts, 15,000 ft flight condition, and get a Level 1 (HQR 3) rating. The pilots commented that it was “easy to attain adequate performance” and that there was “no noticeable difference between 250 kts and 300 kts.”

Both pilots agreed that their Level 2 performance on the sum-of-sines tracking task was not a good representation of the handling qualities of the control laws, however, and that this task is not well-suited to assess business jet control laws. Despite this, the sum-of-sines tracking task remains an aggressive task intended to exercise the control system in a high-gain pilot-in-the-loop fashion to *expose potential handling qualities cliffs or PIO tendencies, neither of which were encountered in flight.*

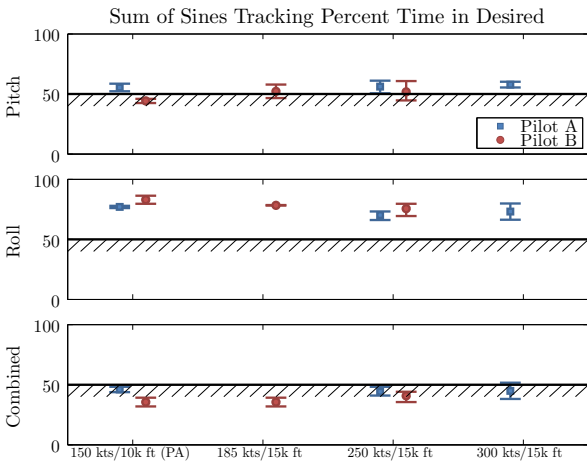


Figure 40. Sum-of-sines tracking task performance.

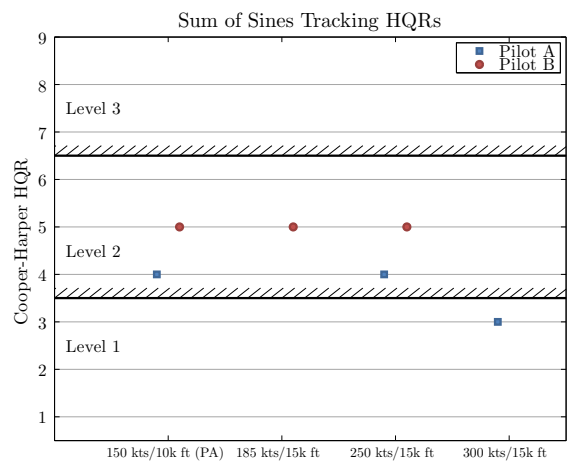


Figure 41. Sum-of-sines tracking HQRs.

4. Offset Precision Landing

Offset landing is a widely used task to evaluate precise handling qualities. It is recommended in MIL-STD-1797B⁶ and WL-TR-97-3100,¹² and is widely used in handling-qualities research studies (e.g., Ref. 25, Ref. 26, Ref. 27).

For this evaluation, pilots initially performed a straight-in approach, then a straight-in precision landing, and finally offset precision landings, with HQRs collected for both straight-in and offset landing tasks. Offset landings were flown with a 200 ft lateral offset on a normal glideslope.

The landing task is divided into two phases—approach and touchdown. The approach phase evaluates the ability to control flight path, airspeed, and attitude. The touchdown phase evaluates the ability to control airspeed, sink rate, and attitude to a precise touchdown, and began at about 50 ft AGL. The pilots attempted to land with the main wheels inside a designated touchdown zone (shown in Figure 42) at a specified sink rate. Table 5 lists detailed desired and adequate performance objectives for the tasks, based on MIL-STD-1797B.

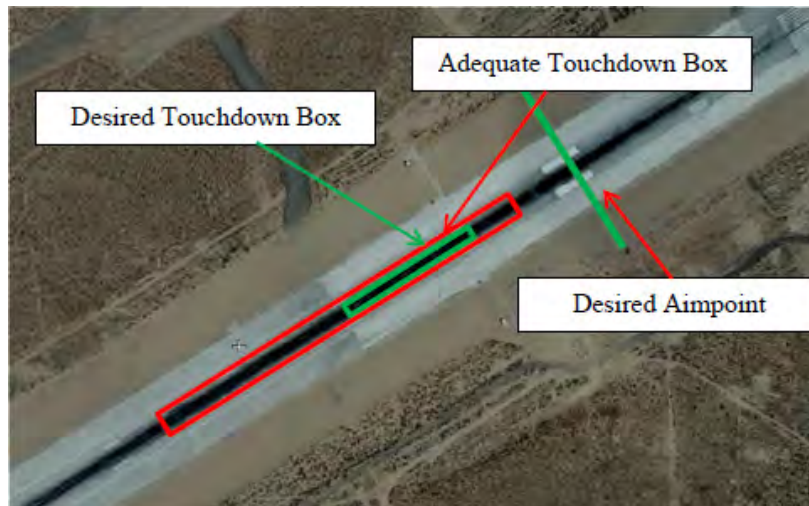


Figure 42. Landing task touchdown box.

Table 5. Performance Criteria - Offset Landing

	Desired	Adequate
<i>Approach</i>		
Remain within X degrees of glideslope angle	±1 deg	±2 deg
Remain within X kts of approach speed	±5 kts	±10 kts
No PIO	✓	NA
<i>Flare/Touchdown</i>		
Within X ft of aim point laterally	±10 ft	±20 ft
Within X ft of aim point longitudinally	-250 to +1000 ft	-500 to +1750 ft
Within X kts of approach speed at flare initiation	±5 kts	±10 kts
Sink rate at touchdown	No bounce/smooth touchdown	No more than 1 bounce/not a hard touchdown
No PIO	✓	NA

Landing tasks were performed by both the Textron Aviation test pilots and the USAF IPs, using only the advanced FBW control laws. As mentioned above, pilots first performed straight-in low approaches, then straight-in precision landings, and finally offset precision landings.

The Textron Aviation pilots flew the landings on a calm day, and provided comments only (no HQRs) on the advanced FBW control laws. The first Textron Aviation pilot commented that the closed-loop aircraft was a “fairly easy airplane to land” and that “pitch and roll control was good.” Commenting on the lateral offset correction with the advanced FBW control laws, the pilot said that “correcting the offset was easy,” that he “was able to smoothly correct to center line prior to reaching the threshold,” and that “no rudder input was necessary to coordinate the turn” as provided by the sideslip-command directional axis control laws. He also noted that “control in the flare was good although there is a tendency to float.”

The second Textron Aviation pilot commented that “controllability in the offset [was] very good” and that the “flare felt normal.” The third Textron Aviation pilot commented that the airplane with the FBW control laws was “business-jet like” and that correcting the “offset was easy.” These comments (especially from pilots so familiar with business jets) indicate that the closed-loop handling characteristics exhibit classical airplane response types that did not require pilot re-training or adaptation.

The USAF IPs flew the landing tasks on a windier day, and provided both comments and HQRs for the landing tasks. Pilot A commented that with the advanced FBW control laws, on the straight-in low approach he was “essentially hands off” and that it was “very stable on final.” Furthermore, on the straight-in precision landing, Pilot A commented that the aircraft was “very stable” and “very easy to fly,” and rated the task an HQR 1 based on the very low workload (Figure 43).

The USAF IP Pilot A flew the offset landing task four times, and was able to attain desired performance on all four runs. Pilot A commented that with the advanced FBW control laws, the lateral axis was “very predictable” and that the task required “minimal compensation.” The pilot rated the four runs HQR 2, HQR 3, HQR 2, and HQR 2 (Figure 43). At the end of Pilot A’s flight, the safety pilot (SP) landed the aircraft flying the baseline, open-loop Learjet. After that landing, Pilot A commented that it was “amazing how much harder [the SP with direct mode was] working to land than [he] was” with the advanced FBW control laws.

Pilot B did not perform any touchdowns due the high crosswinds during the time of his evaluations (25 kts gusting to 30 kts) being outside the VSS landing envelope. However, Pilot B did perform two low approaches in the crosswinds and noted that for the advanced FBW control laws his “feet were not active” and that the airplane was “very stable.”

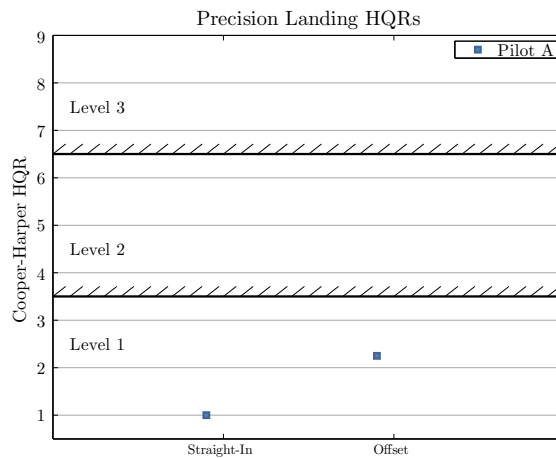


Figure 43. Precision landing HQRs.

5. General Comments

The following is a collection of general comments from the three Textron Aviation pilots who tested the advanced FBW control laws:

- “The control laws were stable and smooth in all three axes, and the aircraft was flown through a large part of the low altitude envelope including landings without significant issues.”
- “Airplane flies very similarly fast/slow and clean/dirty.”
- “The control laws overcame the natural pitch bobble of the basic Learjet mode” (after flying the control laws back to back with the baseline Learjet). This demonstrates the reduced pitch attitude dropback of the control laws as compared to the baseline Learjet.
- With the control laws engaged, “very easy to control and holds well,” while open-loop (baseline Learjet) when you “make a change, [you] have to stay in the loop to control it.”
- The pitch axis was “very stable and forgiving.”
- “The control laws were smooth and stable” in roll.
- “No tendency to overbank during windup turns.”
- “Force increase felt linear and speed control was predictable. Roll control was easy with no tendency to overshoot” during windup turn maneuver.
- “Entry into steady heading sideslip was predictable and smooth.”

These comments are all consistent with the good damping, stability, and robust performance that the control laws were designed to have.

V. Conclusions

A handling-qualities specification driven, multi-objective parametric optimization approach to flight control design was used to develop advanced FBW control laws for a business jet using CONDUIT[®]. An explicit model following architecture was used which provides an $n_z u$ -command response type in the longitudinal axis and a p - β -command response type in the lateral/directional axes. The control laws were tuned for, and then implemented on, the Calspan VSS Learjet-25, and a handling qualities flight-test assessment was performed. The following conclusions are suggested by the flight-test results:

1. The lateral axis command-model time constant was reduced based on initial testing and pilot comments. The updated gain schedule resulted in designs which are more aggressive than the Level 1 Category A MIL-STD-1797B requirements for equivalent roll mode time constant and bandwidth/phase delay. In addition, pitch and roll stick gains were increased to be more similar to the baseline, open-loop Learjet configuration.

2. The implementation of the FBW control laws on the Learjet’s Variable Stability System, as well as the analysis model used to design the control laws, were validated by performing dynamic checks in flight. Closed-loop piloted frequency sweeps and broken-loop automated frequency sweeps were used to produce frequency response overlays between flight data and the analysis model. The frequency responses matched well in all axes, validating the stitched model used in the control law design and control law implementation.
3. The sum-of-sines tracking tasks received Level 2 HQRs, however pilots agreed this task was not well-suited to assess business jet control system handling qualities. Handling-qualities “cliff” or PIO tendencies were not exposed even for this very aggressive task.
4. The FBW control laws received assigned Level 1 HQRs for discrete tracking and offset landing tasks. When compared to the bare-airframe, pilot comments suggested that the FBW control laws provided better precision and improved workload. In addition, the control laws exhibited classical airplane response types that did not require any pilot adaptation.
5. The performance of the FBW control laws validates the specification-driven multi-objective optimization approach to flight control design used to develop the control laws. Tier 1 specifications were used in the optimization to design control laws at 92 total flight conditions with predicted Level 1 handling qualities, while Tier 2 specifications were used as a check upon completion of the optimization.
6. Performance and HQRs did not vary significantly with flight condition or aircraft loading configuration, thus validating the performance robustness of the control laws designed by using a multi-model optimization approach and by enforcing a minimum crossover frequency in each control law axis.

Acknowledgments

The authors would like to sincerely thank all the people who contributed to making this flight test a success: Jason Kirkpatrick, Ryan McMahon, Evan Thomas, Jim Hinline, and Paul Deppe (Calspan Corporation); Scott Foster, Peter Fisher, and Ken Lieber (Textron Aviation); and Maj Stephen Koether and Dave Evans (USAF TPS).

References

- ¹Anon., “Flight Control Design - Best Practices,” NATO RTO-TR-029, December 2000.
- ²Pratt, R. W., “Flight Control Systems,” AIAA Progress in Astronautics and Aeronautics, Vol. 184, 2000.
- ³Tischler, M. B., Berger, T., Ivler, C. M., Mansur, Mohammadreza, H., Cheung, K. K., and Soong, J. Y., *Practical Methods for Aircraft and Rotorcraft Flight Control Design: An Optimization Based Approach*, AIAA, 2017.
- ⁴Mitchell, D. G., Hoh, R. H., L., A. B., and H., K. D., “Proposed Incorporation of Mission-Oriented Flying Qualities into MIL STD-1797A,” Report No. WL-TR-94-3162. Wright-Patterson Air Force Base, Ohio: Wright Laboratory, October 1994.
- ⁵Gibson, J. C., “Development of a Design Methodology for Handling Qualities Excellence in Fly by Wire Aircraft,” Delft University Press, February 1999.
- ⁶Anon., “Flying Qualities of Piloted Aircraft,” MIL-STD-1797B, Department of Defense Interface Standard, February 2006.
- ⁷Balas, G. G. and Hodgkinson, J., “Control Design Methods for Good Flying Qualities,” presented at the AIAA Atmospheric Flight Mechanics Conference, Chicago, IL, August 2009.
- ⁸Berger, T., Tischler, M. B., Hagerott, S. G., Gangsaas, D., and Saeed, N., “Longitudinal Control Law Design and Handling Qualities Optimization for a Business Jet Flight Control System,” presented at the AIAA Atmospheric Flight Mechanics Conference, Minneapolis, MN, August 2012.
- ⁹Berger, T., Tischler, M. B., Hagerott, S. G., Gangsaas, D., and Saeed, N., “Lateral/Directional Control Law Design and Handling Qualities Optimization for a Business Jet Flight Control System,” presented at the AIAA Atmospheric Flight Mechanics Conference, Boston, MA, August 2013.
- ¹⁰Berger, T., Tischler, M. B., and Hagerott, S. G., “Piloted Simulation Handling Qualities Assessment of a Business Jet Fly-By-Wire Flight Control System,” presented at the AIAA Atmospheric Flight Mechanics Conference, Kissimmee, FL, January 2015.
- ¹¹Tischler, M. B., Ivler, C. M., Mansur, M. H., Cheung, K. K., Berger, T., and Berrios, M., “Handling-Qualities Optimization and Trade-offs in Rotorcraft Flight Control Design,” presented at the Rotorcraft Handling Qualities Conference, University of Liverpool, UK, November 2008.
- ¹²Klyde, D. H. and Mitchell, D. G., “Handling Qualities Demonstration Maneuvers for Fixed-Wing Aircraft, Volume II: Maneuver Catalog,” WL-TR-97-3100, October 1997.

- ¹³Tobias, E. L. and Tischler, M. B., "A Model Stitching Architecture for Continuous Full Flight-Envelope Simulation of Fixed-Wing Aircraft and Rotorcraft from Discrete-Point Linear Models," U.S. Army AMRDEC Special Report RDMR-AF-16-01, April 2016.
- ¹⁴Berger, T., Tischler, M. B., Hagerott, S. G., Cotting, M. C., Gresham, J. L., George, J. E., Krogh, K. J., D'Argenio, A., and Howland, J. D., "Development and Validation of a Flight Identified Business Jet Simulation Model Using a Stitching Architecture," AIAA Modeling and Simulation Technologies Conference, Grapevine, TX, January 2017.
- ¹⁵Anon., "Type Certificate Data Sheet No. A10CE Rev. 47," Department of Transportation Federal Aviation Administration, 1995.
- ¹⁶Stevens, B. L. and Lewis, F. L., *Aircraft Control and Simulation Second Edition*, Wiley, 2003.
- ¹⁷Gangsaas, D., Hodgkinson, J., Harden, C., Saeed, N., and Chen, K., "Multidisciplinary Control Law Design and Flight Test Demonstration on a Business Jet," presented at the AIAA Guidance, Navigation, and Control Conference and Exhibit, Honolulu, HI, August 2008.
- ¹⁸Adams, R. J., Buffington, J. M., Sparks, A. G., and Banda, S. S., *Robust Multivariable Flight Control*, Springer-Verlag, 1994.
- ¹⁹Blight, J. D., Calderia, F. R., and Gangsaas, D., "Control Law Development for Aircraft An Example of Industry Practices," presented at the American Control Conference, Seattle, WA, June 2008.
- ²⁰Anon., "Airworthiness Standards: Transport Category Airplanes," Code of Federal Regulations, Title 14, Part 25, Department of Transportation Federal Aviation Administration, January 2004.
- ²¹Anon., "Aerospace - Flight Control Systems - Design, Installation and Test of Piloted Military Aircraft, General Specification For," SAE-AS94900, July 2007.
- ²²Gresham, J. L., George, J. E., Krogh, K. J., D'Argenio, A., and Howland, J. D., "Limited Evaluation of Cessna Aircraft Company Control Law (Project Tacit CLEAR)," USAF TPS-TIM-15B-02, June 2016.
- ²³Tischler, M. B. and Remple, R. K., *Aircraft and Rotorcraft System Identification: Engineering Methods and Flight Test Examples Second Edition*, AIAA, 2012.
- ²⁴Cooper, G. and Harper, Jr., R., "The Use of Pilot Rating in the Evaluation of Aircraft Handling Qualities," NASA TN D5153, April 1969.
- ²⁵Field, E. J., Armor, J. B., Rossitto, K. F., and Mitchell, D. G., "Effects of Pitch Instantaneous Center of Rotation Location on Flying Qualities," AIAA Atmospheric Flight Mechanics Conference, Monterey, CA, August 2002.
- ²⁶Klyde, D. H. and Liang, C.-Y., "Approach and Landing Flight Evaluation of Smart-Cue and Smart-Gain Concepts," AIAA Journal of Guidance, Control, and Dynamics, Vol. 32, No. 4, July-August 2009.
- ²⁷Stroosma, O., Damveld, H. J., Mulder, J. A., Choe, R., Xargay, E., and Hovakimyan, N., "A Handling Qualities Assessment of a Business Jet Augmented with an \mathcal{L}_1 Adaptive Controller," AIAA Guidance, Navigation, and Control Conference, Portland, OR, August 2011.